

Spherical nano-inhomogeneity with Steigmann–Ogden interface model under general uniform far-field stress

Junbo Wang¹, Peng Yan^{1*}, Leiting Dong^{1*}

¹School of Aeronautic Science and Engineering, Beihang University, Beijing 100191,
CHINA

Abstract: An explicit analytical solution considering interface bending resistance based on the Steigmann–Ogden interface model is derived for a spherical nano-inhomogeneity (nanoscale void/inclusion) embedded in an infinite matrix under general uniform far-field stress (including both tension and shear). The Papkovitch–Neuber (P-N) general solutions, which are expressed in terms of spherical harmonics, are used to derive the analytical solution. A superposition technique for the Steigmann–Ogden interface model is introduced to overcome the mathematical complexity in the Steigmann–Ogden interface model, that is the nonlinearity of the constitutive relation brought by interface residual stress. Numerical examples show that the stress fields considering the interface bending resistance with the Steigmann–Ogden interface model, differ a lot from those considering only the interface stretching resistance with the Gurtin–Murdoch interface model, when

* Corresponding author: yanpeng117@buaa.edu.cn (P. Yan). Address: School of Aeronautic Science and Engineering, Beihang University, Beijing, 100191, CHINA.

* Corresponding author: ltdong@buaa.edu.cn (L. Dong). Address: School of Aeronautic Science and Engineering, Beihang University, Beijing, 100191, CHINA.

interface bending parameters get closed to the characteristic line introduced in this study. In addition to size-dependency phenomenon, it is also observed that some stress components are invariant to interface bending stiffness parameters at a certain circle in the inclusion/matrix. A characteristic line for the interface bending stiffness parameters is presented, near which the stress concentration phenomenon becomes quite severe. The derived explicit analytical solution with the Steigmann–Ogden interface model can be used as a benchmark for semi-analytical solutions and numerical solutions.

Keywords: Steigmann–Ogden interface model; spherical nano-inhomogeneity; general uniform far-field stress; analytical solution

1. Introduction

The interface stress theory has attracted much attention due to its potential applicability to nanocomposites and nanostructure materials. The concept of interface stress was first introduced by Gibbs (1906) and has been extensively investigated since Gurtin and Murdoch (1975, 1978) incorporated interface stress into continuum mechanics. In the Gurtin–Murdoch model, the interface is considered as a negligibly thin layer adhering to bulk materials without slipping, and have only stretching resistance but no bending resistance. Gurtin et al. (1998) generalized the original model by allowing all the components of the displacement vector to undergo a jump across the interface. The Gurtin–Murdoch model has been used to study nanosized rod (e.g. Altenbach et al., 2013a; Altenbach et al., 2013b), beams (e.g. Miller and Shenoy, 2000b;

Eltaher et al., 2013; Ansari et al., 2015; Youcef et al., 2018), plates (e.g. Eremeyev et al., 2009; Ansari and Sahmani, 2011; Altenbach et al., 2012; Ansari and Norouzzadeh, 2016), shells (e.g. Altenbach et al., 2010; Altenbach and Eremeyev, 2011; Rouhi et al., 2016; Sahmani et al., 2016), films (e.g. Lu et al., 2011; Zhao and Rajapakse, 2013), wires (e.g. Diao et al., 2003; He and Lilley, 2008; Yvonnet et al., 2011), and inhomogeneities (e.g. Sharma et al., 2003; He and Li, 2006; Lim et al., 2006; Mogilevskaya et al., 2008; Mogilevskaya et al., 2010; Kushch et al., 2011; Kushch et al., 2013; Mi and Kouris, 2014; Nazarenko et al., 2016), and much progress has been achieved in both analytical methods (e.g. Mogilevskaya et al., 2008; Duan et al., 2009; Altenbach et al., 2013a; Kushch et al., 2013; Dong et al., 2018) and numerical methods (e.g. Tian and Rajapakse, 2007; Feng et al., 2010; Dong and Pan, 2011). All these studies show the interface stress has remarkable influences on elastic fields and overall properties of the nanosize materials and structures.

In the Gurtin-Murdoch model, the surface/interface energy only depends on the surface/interface strains and the residual surface stress, thus the material interfaces are assumed to have only stretching resistance but no bending resistance. This leads the Gurtin–Murdoch model being unable to account for the experimental observations and calculation results of the size-dependence of the surface stresses for nanowires (McDowell et al., 2008; Yun and Park, 2009), nanoplates (Miller and Shenoy, 2000a) and nanoparticles (Medasani et al., 2007) because the curvature elastic energy of the surface is neglected. Steigmann and Ogden (1997, 1999) pointed out that the membrane

in the Gurtin–Murdoch model cannot support compressive stress states, thus cannot simulate surface features characterized by compressive surface stresses of any magnitude such as surface wrinkling and roughening. In order to overcome such deficiencies, Steigmann and Ogden (1999) generalized the Gurtin–Murdoch model to take into account both stretching and bending resistance of the membrane. The variational framework for the derivations of the basic equations for the model was first presented by Eremeyev and Lebedev (2016). Subsequently, Zemlyanova and Mogilevskaya (2018a) clarified the derivations of the governing equations in that paper, and corrected some misprints of the final expressions. They presented the corresponding equations for the model in a particularly accessible form and they did it for general three-dimensional case, which is for the complete model with surface tension. These equations have been used in all subsequent publications on the topic (Zemlyanova, 2017, 2018a, b; Zemlyanova and Mogilevskaya, 2018b), and will be used in this study.

In contrast to the popularity of the Gurtin–Murdoch model, the Steigmann–Ogden model has received less attention so far. Most literatures on the Steigmann–Ogden model are focused on nanosized materials and structures with simple geometry shapes, such as nanobeams (Chhapadia et al., 2011; Manav et al., 2018), nanowires (Zhao et al., 2015), rigid stamps (Zemlyanova, 2018a, b), thin films (Ogden et al., 1997; Dryburgh and Ogden, 1999) and half-space materials (Li and Mi, 2018; Mi, 2018). Literatures on nano-porous material and nano-particle reinforced composites considering the

Steigmann–Ogden surface elasticity model are rather limited (Gharahi and Schiavone, 2018; Han et al., 2018; Zemlyanova and Mogilevskaya, 2018a, b), and most of these studies are focused on 2D nano-inhomogeneity problems. Among these studies, Zemlyanova, Mogilevskaya (2018a) derived analytical solutions to the plane strain problem of an infinite isotropic elastic domain containing an isotropic elastic circular inhomogeneity. Han et al. (2018) presented a semi-analytical solution of transverse local fields and overall transverse properties of composite materials with aligned multiple cylindrical nanofibers. The only paper dealing with 3D problems is presented by Zemlyanova and Mogilevskaya (2018b), in which two special solutions are derived for the problems under the hydrostatic loading and deviatoric loading with vanishing surface tension. These studies show that the interface bending resistance may significantly affect both the stress concentrations in the local fields and the effective properties of materials when the inclusion is nano-sized. However, though Zemlyanova and Mogilevskaya (2018b) have found analytical solutions for 2 special boundary conditions, for 3D nano-inhomogeneities problems under arbitrary remote loading, due to the mathematical complexity brought by the interface bending and residual stress, studies based on the Steigmann-Ogden interface model have not been reported to the best of our knowledge. Especially, an analytical solution for a spherical nano-inhomogeneity, which can serve as a benchmark for numerical solutions, is very desirable.

In this study, a superposition technique is introduced to overcome the mathematical

complexity in the Steigmann-Ogden interface model, that is the nonlinearity of the constitutive relation brought by interface bending and residual stress . Thereby, an analytical solution considering interface bending resistance based on the Steigmann-Ogden interface model is derived for the first time, for a spherical nano-inhomogeneity (nanoscale void/inclusion) embedded in an infinite matrix under general uniform far-field stress. The rest of this paper is organized as follows: In Section 2, the governing equations for the 3D nano-inhomogeneity with Steigmann-Ogden interface are briefly stated. In Section 3, the Papkovitch-Neuber solutions to the governing equations and the expression with spherical harmonics are detailed. Then combining with the Steigmann-Ogden interface condition and the far-field condition, the explicit analytical solution to the considered nano-inhomogeneity problem is given in Section 4. In Section 5, we discuss the effects of the interface bending on stress distributions within and around the nano-inhomogeneities (nano-void/inclusion), when the far-field tensile/shear loadings are applied. In Section 6, we complete this paper with some concluding remarks.

2. The governing linear elasticity equations

The problem of a nano-inhomogeneity embedded in an infinite matrix subjected to a general uniform far-field stress is considered, as shown in Fig. 1. Solutions of 3D linear elasticity for the matrix and the inhomogeneity should satisfy the equations of stress equilibrium, strain displacement-gradient compatibility, as well as the constitutive relations in each domain Ω^j :

$$\nabla \cdot \boldsymbol{\sigma}^j + \mathbf{f}^j = 0 \quad (1)$$

$$\boldsymbol{\varepsilon}^j = \frac{1}{2}(\nabla \mathbf{u}^j + (\nabla \mathbf{u}^j)^T) \quad (2)$$

$$\boldsymbol{\sigma}^j = \lambda^j \text{tr}(\boldsymbol{\varepsilon}^j) \mathbf{I}_3 + 2\mu^j \boldsymbol{\varepsilon}^j \quad (3)$$

where the superscript $j = m$ denotes the matrix domain, and $j = i$ denotes the inhomogeneity domain. $\boldsymbol{\sigma}^j$, $\boldsymbol{\varepsilon}^j$, \mathbf{u}^j are stresses, strains, and displacements in matrix/inhomogeneity. \mathbf{f}^j is the body force in matrix/ inhomogeneity, which does not appear in the problem considered here. $\nabla \cdot$ and ∇ are the divergence and gradient operators, respectively. $\lambda^j = \frac{\nu^j E^j}{(1-2\nu^j)(1+\nu^j)}$ and $\mu^j = \frac{E^j}{2(1+\nu^j)}$ are Lamé constants for matrix/inclusion, where E^j and ν^j are the Young's modulus and Poisson's ratio, respectively. \mathbf{I}_3 is the 3D unit tensor and $\mathbf{I}_3 = \mathbf{e}_r \otimes \mathbf{e}_r + \mathbf{e}_\theta \otimes \mathbf{e}_\theta + \mathbf{e}_\varphi \otimes \mathbf{e}_\varphi$ in spherical coordinates, where \mathbf{e}_r , \mathbf{e}_θ , \mathbf{e}_φ are base vectors. $\text{tr}(\boldsymbol{\varepsilon}^j)$ denotes the trace of the strain tensor.

A general uniform far-field stress loading, prescribed as a boundary condition, can be arbitrary combination of shear and tension, and can be written as:

$$\boldsymbol{\sigma}^m = \boldsymbol{\sigma}^0 \quad \text{at infinity} \quad (4)$$

The component form is $\boldsymbol{\sigma}^0 = \begin{pmatrix} \sigma_{xx}^0 & \sigma_{xy}^0 & \sigma_{xz}^0 \\ \sigma_{xy}^0 & \sigma_{yy}^0 & \sigma_{yz}^0 \\ \sigma_{xz}^0 & \sigma_{yz}^0 & \sigma_{zz}^0 \end{pmatrix}$, which includes both normal stresses

and shear stresses in general.

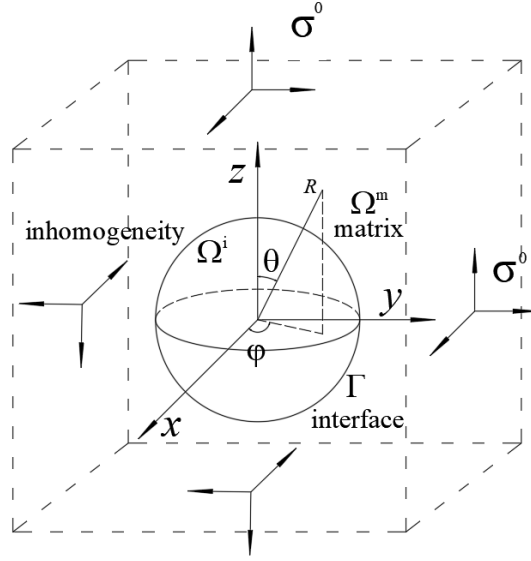


Fig. 1. A spherical inhomogeneity embedded in an infinite matrix under far-field stress loading

The Steigmann–Ogden interface model is applied to consider the bending resistance, as well as interface stretching resistance and residual stress. Derivation of the Steigmann–Ogden interface model is detailed in Zemlyanova and Mogilevskaya (2018a), and is summarized in the following. In this model, the interface between the matrix and the inhomogeneity has its own Lamé constants, and its elastic response is governed the following equations. The displacement across the interface is continuous,

$$\mathbf{u}^m = \mathbf{u}^i \text{ at } \Gamma \quad (5)$$

The stress across the interface has a jump,

$$\mathbf{n} \cdot \Delta \boldsymbol{\sigma} = \nabla_s \cdot [\boldsymbol{\tau}^s + (\nabla_s \cdot \mathbf{m}^s) \mathbf{n}] - (\nabla_s \cdot \mathbf{n}) \mathbf{n} \cdot (\nabla_s \cdot \mathbf{m}^s) \mathbf{n} \text{ at } \Gamma \quad (6)$$

The constitutive equation of the interface is

$$\boldsymbol{\tau}^s = \sigma^s \mathbf{I}_s + 2(\mu^s - \sigma^s) \boldsymbol{\varepsilon}^s + (\lambda^s + \sigma^s) \text{tr}(\boldsymbol{\varepsilon}^s) \mathbf{I}_s + \sigma^s \nabla_s \mathbf{u}^s \quad (7)$$

$$\mathbf{m}^s = 2\chi^s \boldsymbol{\kappa}^s + \zeta^s \text{tr}(\boldsymbol{\kappa}^s) \mathbf{I}_s \quad (8)$$

where

$$\boldsymbol{\varepsilon}^s = \frac{1}{2} \left[\nabla_s \mathbf{u}^s \cdot \mathbf{I}_s + \mathbf{I}_s \cdot (\nabla_s \mathbf{u}^s)^T \right] \quad (9)$$

$$\boldsymbol{\kappa}^s = -\frac{1}{2} \left[\nabla_s \mathcal{G} \cdot \mathbf{I}_s + \mathbf{I}_s \cdot (\nabla_s \mathcal{G})^T \right] \quad (10)$$

$$\mathcal{G} = \nabla_s (\mathbf{n} \cdot \mathbf{u}^s) + \mathbf{B} \cdot \mathbf{u}^s \quad (11)$$

$$\mathbf{B} = -\nabla_s \mathbf{n} \quad (12)$$

where $\mathbf{u}^s, \boldsymbol{\varepsilon}^s, \boldsymbol{\tau}^s, \boldsymbol{\kappa}^s$ and \mathbf{m}^s are interface displacement, strain, stress, curvature and bending moment tensors, respectively. λ^s and μ^s are the interface Lamé constants characterizing the interface stretching. χ^s and ζ^s are stiffness parameters characterizing the interface bending. σ^s is the residual surface stress. \mathbf{I}_s is the unit tangent tensor defined on the interface and $\mathbf{I}_s = \mathbf{e}_\theta \otimes \mathbf{e}_\theta + \mathbf{e}_\varphi \otimes \mathbf{e}_\varphi$ in spherical coordinates. $\nabla_s = (\mathbf{I}_3 - \mathbf{n}\mathbf{n}) \cdot \nabla$ is the gradient operator defined on the interface where \mathbf{n} is the unit outer-normal vector of the interface Γ .

3. Papkovitch-Neuber solutions with spherical harmonics

3.1. Papkovitch-Neuber solutions

In order to solve the governing equations Eqs. (1-3), Navier's equation

$$(\lambda^j + \mu^j) \nabla (\nabla \cdot \mathbf{u}^j) + \mu^j \nabla^2 \mathbf{u}^j + \mathbf{f}^j = 0 \quad (13)$$

is derived Lurie (2005). The solutions of Navier's equation can be represented in the forms of harmonic functions (Papkovitch, 1932; Neuber, 1934; Lurie, 2005) when the body force is neglected:

$$\mathbf{u}^j = [4(1-\nu^j)\mathbf{B}^j - \nabla(\mathbf{R} \cdot \mathbf{B}^j + B_0^j)] / 2\mu^j \quad (14)$$

where B_0^j and $\mathbf{B}^j = [B_1^j \ B_2^j \ B_3^j]^T$ are scalar and vector harmonic functions. \mathbf{R} is the position vector.

According to Slobodyansky (1954), by dropping B_0^k the following solution:

$$\mathbf{u}^j = [4(1-\nu^j)\mathbf{B}^j - \nabla\mathbf{R} \cdot \mathbf{B}^j] / 2\mu^j \quad (15)$$

is complete for an infinite domain external to a closed surface (Slobodyansky, 1954), thus will be applied in the matrix domain. However, for a simply-connected domain, Eq.(15) is incomplete when $\nu^j = 0.25$. Therefore, according to Slobodyansky (1954), another general solution,

$$\mathbf{u}^j = [4(1-\nu^j)\mathbf{B}^j + \mathbf{R} \cdot \nabla\mathbf{B}^j - \mathbf{R}\nabla \cdot \mathbf{B}^j] / 2\mu^j \quad (16)$$

is obtained by expressing B_0^j in Eq.(14) as a specific function of \mathbf{B}^j . This general solution is complete for any Poisson ratio ν^j in a simply connected domain, thus will be applied in the inclusion domains.

3.2. Spherical harmonics

The displacement field in the inclusion can be derived by substituting the non-singular harmonics:

$$\mathbf{B}_p^i = \sum_{n=0}^{\infty} R^n \left\{ \mathbf{a}_0^i YC_0^0(\theta, \varphi) + \sum_{l=1}^n [\mathbf{a}_n^l YC_n^l(\theta, \varphi) + \mathbf{b}_n^l YS_n^l(\theta, \varphi)] \right\} \quad (17)$$

into Eq.(16):

$$\mathbf{u}^i = \mathbf{u}_p^i = [4(1-\nu^i)\mathbf{B}_p^i + \mathbf{R} \cdot \nabla\mathbf{B}_p^i - \mathbf{R}\nabla \cdot \mathbf{B}_p^i] / 2\mu^i \quad (18)$$

where \mathbf{a}_n^i , \mathbf{b}_n^i are the unknown coefficients to be determined. $YC_n^l(\theta, \varphi)$ and

$YS_n^l(\theta, \varphi)$ are spherical harmonics:

$$\begin{aligned} YC_n^l(\theta, \varphi) &= \sqrt{\frac{2n+1}{4\pi} \frac{(n-l)!}{(n+l)!}} P_n^l(\cos(\theta)) \cos(k\varphi) \\ YS_n^l(\theta, \varphi) &= \sqrt{\frac{2n+1}{4\pi} \frac{(n-l)!}{(n+l)!}} P_n^l(\cos(\theta)) \sin(k\varphi) \\ P_n^l(x) &= \frac{(1-x^2)^{\frac{l}{2}}}{2^n n!} \frac{d^{n+l}}{dx^{n+l}} (x^2-1)^n \end{aligned} \quad (19)$$

The displacement field in the matrix is the summation of \mathbf{u}_p^m (the non-singular part) and \mathbf{u}_k^m (the singular part, with the singularity located at the centre of the inclusion). \mathbf{u}_p^m can be derived by substituting

$$\mathbf{B}_p^m = \sum_{n=0}^{\infty} R^n \left\{ \mathbf{c}_0^0 YC_0^0(\theta, \varphi) + \sum_{l=1}^n \left[\mathbf{c}_n^l YC_n^l(\theta, \varphi) + \mathbf{d}_n^l YS_n^l(\theta, \varphi) \right] \right\} \quad (20)$$

into Eq.(16), and \mathbf{u}_k^m can be derived by substituting

$$\mathbf{B}_k^m = \sum_{n=0}^{\infty} R^{-(n+1)} \left\{ \mathbf{s}_0^0 YC_0^0(\theta, \varphi) + \sum_{l=1}^n \left[\mathbf{s}_n^l YC_n^l(\theta, \varphi) + \mathbf{t}_n^l YS_n^l(\theta, \varphi) \right] \right\} \quad (21)$$

into Eq. (15):

$$\begin{aligned} \mathbf{u}^m &= \mathbf{u}_p^m + \mathbf{u}_k^m \\ \mathbf{u}_p^m &= \left[4(1-\nu^m) \mathbf{B}_p^m + \mathbf{R} \cdot \nabla \mathbf{B}_p^m - \mathbf{R} \nabla \cdot \mathbf{B}_p^m \right] / 2\mu^m \\ \mathbf{u}_k^m &= \left[4(1-\nu^m) \mathbf{B}_k^m - \nabla \mathbf{R} \cdot \mathbf{B}_k^m \right] / 2\mu^m \end{aligned} \quad (22)$$

where $\mathbf{s}_n^l, \mathbf{t}_n^l, \mathbf{c}_n^l, \mathbf{d}_n^l$ are the unknown coefficients.

4. Solution to the problem by a new superposition technique

By employing Papkovitch–Neuber solutions, the elastic field caused by the general uniform far-field stress is obtained explicitly. First, we consider the case that the remote loading has only one non-zero stress component σ_{xx}^0 . The unknown coefficients in

equations above can be determined by satisfying Eqs.(4-6). After solving the unknown coefficients, the displacement components of \mathbf{u}_{xx}^j (here we use \mathbf{u}_{st}^j to denote the displacement vector when the remote loading has only one non-zero component σ_{st}^0) can be simplified as:

$$\begin{aligned}
u_{rxx}^m &= M_{1xx}r + \frac{M_{2xx}}{r^2} - \frac{1}{8} \left(2M_{3xx}r + \frac{2(5-4v^m)}{r^2} M_{4xx} - 3 \frac{M_{5xx}}{r^4} \right) (1 + 3 \cos[2\theta] - 6 \cos[2\phi] \sin[\theta]^2) \\
u_{\theta xx}^m &= 3 \left(M_{3xx}r + \frac{2(1-2v^m)}{r^2} M_{4xx} + \frac{M_{5xx}}{r^4} \right) \cos[\theta] \cos[\phi]^2 \sin[\theta]; \\
u_{\phi xx}^m &= -3 \left(M_{3xx}r + \frac{2(1-2v^m)}{r^2} M_{4xx} + \frac{M_{5xx}}{r^4} \right) \cos[\phi] \sin[\theta] \sin[\phi]; \quad (23) \\
u_{rxx}^i &= C_{1xx}r - \frac{1}{8} (12v^i C_{2xx}r^3 + 2C_{3xx}r) (1 + 3 \cos[2\theta] - 6 \cos[2\phi] \sin[\theta]^2); \\
u_{\theta xx}^i &= 3 \left((7-4v^i) C_{2xx}r^3 + C_{3xx}r \right) \cos[\theta] \cos[\phi]^2 \sin[\theta]; \\
u_{\phi xx}^i &= -3 \left((7-4v^i) C_{2xx}r^3 + C_{3xx}r \right) \cos[\phi] \sin[\theta] \sin[\phi];
\end{aligned}$$

By using the same procedure, the displacement components of \mathbf{u}_{yy}^k under the remote tensile stress σ_{yy}^0 can be written as:

$$\begin{aligned}
u_{ryy}^m &= M_{1yy}r + \frac{M_{2yy}}{r^2} - \frac{1}{8} \left(2M_{3yy}r + \frac{2(5-4v^m)}{r^2} M_{4yy} - 3 \frac{M_{5yy}}{r^4} \right) (1 + 3 \cos[2\theta] + 6 \cos[2\phi] \sin[\theta]^2); \\
u_{\theta yy}^m &= 3 \left(M_{3yy}r + \frac{2(1-2v^m)}{r^2} M_{4yy} + \frac{M_{5yy}}{r^4} \right) \cos[\theta] \sin[\theta] \sin[\phi]^2; \\
u_{\phi yy}^m &= 3 \left(M_{3yy}r + \frac{2(1-2v^m)}{r^2} M_{4yy} + \frac{M_{5yy}}{r^4} \right) \cos[\phi] \sin[\theta] \sin[\phi]; \quad (24) \\
u_{ryy}^i &= C_{1yy}r - \frac{1}{8} (12v^i C_{2yy}r^3 + 2C_{3yy}r) (1 + 3 \cos[2\theta] + 6 \cos[2\phi] \sin[\theta]^2); \\
u_{\theta yy}^i &= 3 \left((7-4v^i) C_{2yy}r^3 + C_{3yy}r \right) \cos[\theta] \sin[\theta] \sin[\phi]^2; \\
u_{\phi yy}^i &= 3 \left((7-4v^i) C_{2yy}r^3 + C_{3yy}r \right) \cos[\phi] \sin[\theta] \sin[\phi];
\end{aligned}$$

The displacement components of \mathbf{u}_{zz}^k under the remote tensile stress σ_{zz}^0 can be written as:

$$\begin{aligned}
u_{rzz}^m &= M_{1zz}r + \frac{M_{2zz}}{r^2} + \frac{1}{4} \left(2M_{3zz}r + \frac{2(5-4\nu^m)}{r^2} M_{4zz} - 3\frac{M_{5zz}}{r^4} \right) (1 + 3\cos[2\theta]); \\
u_{\theta zz}^m &= -3 \left(M_{3zz}r + \frac{2(1-2\nu^m)}{r^2} M_{4zz} + \frac{M_{5zz}}{r^4} \right) \cos[\theta] \sin[\theta]; \\
u_{\phi zz}^m &= 0; \\
u_{rzz}^i &= C_{1zz}r + \frac{1}{4} (12\nu^i C_{2zz}r^3 + 2C_{3zz}r) (1 + 3\cos[2\theta]); \\
u_{\theta zz}^i &= -3 \left((7-4\nu^i) C_{2zz}r^3 + C_{3zz}r \right) \cos[\theta] \sin[\theta]; \\
u_{\phi zz}^i &= 0;
\end{aligned} \tag{25}$$

The displacement components of \mathbf{u}_{xy}^k under the remote shear stress σ_{xy}^0 can be written as:

$$\begin{aligned}
u_{rxy}^m &= \frac{M_{2xy}}{r^2} + \frac{3}{2} \left(2M_{3xy}r + \frac{2(5-4\nu^m)}{r^2} M_{4xy} - 3\frac{M_{5xy}}{r^4} \right) \sin[\theta] \sin[\theta] \sin[2\phi]; \\
u_{\theta xy}^m &= \frac{3}{2} \left(M_{3xy}r + \frac{2(1-2\nu^m)}{r^2} M_{4xy} + \frac{M_{5xy}}{r^4} \right) \sin[2\theta] \sin[2\phi]; \\
u_{\phi xy}^m &= 3 \left(M_{3xy}r + \frac{2(1-2\nu^m)}{r^2} M_{4xy} + \frac{M_{5xy}}{r^4} \right) \sin[\theta] \cos[2\phi]; \\
u_{rxy}^i &= C_{1xy}r + \frac{3}{2} (12\nu^i C_{2xy}r^3 + 2C_{3xy}r) \sin[\theta] \sin[\theta] \sin[2\phi]; \\
u_{\theta xy}^i &= \frac{3}{2} \left((7-4\nu^i) C_{2xy}r^3 + C_{3xy}r \right) \sin[2\theta] \sin[2\phi]; \\
u_{\phi xy}^i &= 3 \left((7-4\nu^i) C_{2xy}r^3 + C_{3xy}r \right) \sin[\theta] \cos[2\phi];
\end{aligned} \tag{26}$$

The displacement components of \mathbf{u}_{yz}^k under the remote shear stress σ_{yz}^0 can be written as:

$$\begin{aligned}
u_{ryz}^m &= \frac{M_{2yz}}{r^2} + \frac{3}{2} \left(2M_{3yz}r + \frac{2(5-4v^m)}{r^2} M_{4yz} - 3 \frac{M_{5yz}}{r^4} \right) \sin[2\theta] \sin[\phi]; \\
u_{\theta yz}^m &= 3 \left(M_{3yz}r + \frac{2(1-2v^m)}{r^2} M_{4yz} + \frac{M_{5yz}}{r^4} \right) \cos[2\theta] \sin[\phi]; \\
u_{\phi yz}^m &= 3 \left(M_{3yz}r + \frac{2(1-2v^m)}{r^2} M_{4yz} + \frac{M_{5yz}}{r^4} \right) \cos[\theta] \cos[\phi]; \\
u_{ryz}^i &= C_{1yz}r + \frac{3}{2} (12v^i C_{2yz}r^3 + 2C_{3yz}r) \sin[2\theta] \sin[\phi]; \\
u_{\theta yz}^i &= 3 \left((7-4v^i) C_{2yz}r^3 + C_{3yz}r \right) \cos[2\theta] \sin[\phi]; \\
u_{\phi yz}^i &= 3 \left((7-4v^i) C_{2yz}r^3 + C_{3yz}r \right) \cos[\theta] \cos[\phi];
\end{aligned} \tag{27}$$

The displacement components of \mathbf{u}_{zx}^k under the remote shear stress σ_{zx}^0 can be written as:

$$\begin{aligned}
u_{r zx}^m &= \frac{M_{2zx}}{r^2} + \frac{3}{2} \left(2M_{3zx}r + \frac{2(5-4v^m)}{r^2} M_{4zx} - 3 \frac{M_{5zx}}{r^4} \right) \sin[2\theta] \cos[\phi]; \\
u_{\theta zx}^m &= 3 \left(M_{3zx}r + \frac{2(1-2v^m)}{r^2} M_{4zx} + \frac{M_{5zx}}{r^4} \right) \cos[2\theta] \cos[\phi]; \\
u_{\phi zx}^m &= -3 \left(M_{3zx}r + \frac{2(1-2v^m)}{r^2} M_{4zx} + \frac{M_{5zx}}{r^4} \right) \cos[\theta] \sin[\phi]; \\
u_{r zx}^i &= C_{1zx}r + \frac{3}{2} (12v^i C_{2zx}r^3 + 2C_{3zx}r) \sin[2\theta] \cos[\phi]; \\
u_{\theta zx}^i &= 3 \left((7-4v^i) C_{2zx}r^3 + C_{3zx}r \right) \cos[2\theta] \cos[\phi]; \\
u_{\phi zx}^i &= -3 \left((7-4v^i) C_{2zx}r^3 + C_{3zx}r \right) \cos[\theta] \sin[\phi];
\end{aligned} \tag{28}$$

where M_{pst} ($p=1, \dots, 5$ and $s, t = x, y, z$) and C_{qst} ($q=1, 2, 3$ and $s, t = x, y, z$) are constants given in Appendix A.

For the case that the remote loading is zero, the displacement components of \mathbf{u}_0^k can be written as:

$$\begin{aligned}
u_{r0}^m &= R^3 (1 - 2\nu^i) \sigma^s / (r^2 ((-2 + 4\nu^i) \lambda^s - R(\mu^i + \nu^i \mu^i + 2\mu^m - 4\nu^i \mu^m) \\
&\quad + (-1 + 2\nu^i)(2\mu^s + \sigma^s))); \\
u_{\theta 0}^m &= 0; \\
u_{\phi 0}^m &= 0; \\
u_{r0}^i &= r (-1 + 2\nu^i) \sigma^s / ((2 - 4\nu^i) \lambda^s + R(\mu^i + \nu^i \mu^i + 2\mu^m - 4\nu^i \mu^m) + 2 \\
&\quad \mu^s + \sigma^s - 2\nu^i (2\mu^s + \sigma^s)); \\
u_{\theta 0}^i &= 0; \\
u_{\phi 0}^i &= 0;
\end{aligned} \tag{29}$$

Now we have obtained the basic solutions for a spherical inhomogeneity under six different remote loadings. However, the analytical solution under remote loading σ^0 is not simply an additive combination of the above Eqs.(22-28), because the linear superposition law for solutions in the classical linear elasticity no longer hold on due to the existence of $\sigma^s \mathbf{I}_s$ in Eq.(7) (see Mogilevskaya et al., 2010; Kushch et al., 2013; Zemlyanova and Mogilevskaya, 2018b). If we simply add Eqs.(22-28) together, the interface stress will be:

$$\boldsymbol{\tau}^s = 6\sigma^s \mathbf{I}_s + 2(\mu^s - \sigma^s) \boldsymbol{\varepsilon}^s + (\lambda^s + \sigma^s) \text{tr}(\boldsymbol{\varepsilon}^s) \mathbf{I}_s + \sigma^s \nabla_s \mathbf{u}^s \tag{30}$$

Obviously, extra 5 terms of $\sigma^s \mathbf{I}_t$ should be eliminated by subtracting the solution with no remote loadings, thus the analytical solution under general remote loading σ^0 should be written as:

$$\mathbf{u}^j = \mathbf{u}_{xx}^j + \mathbf{u}_{yy}^j + \mathbf{u}_{zz}^j + \mathbf{u}_{xy}^j + \mathbf{u}_{yz}^j + \mathbf{u}_{zx}^j - 5\mathbf{u}_0^j \quad j = m, i \tag{31}$$

It can be easily proved that the displacement solution (Eq.(31)) given by the new superposition technique satisfies the governing equations by substituting Eq.(31) into Eqs.(1-6). The solution Eq.(31) reveals that the interface effect is size dependent and different interface properties will have influence on the stress concentration. If the

interface stress is ignored ($\lambda^s = 0$, $\mu^s = 0$, $\sigma^s = 0$, $\chi^s = 0$ and $\zeta^s = 0$), Eq.(31) can be degenerated into the classical Eshelby solutions without interface stress and the size effect no longer exists. If the surface bending resistance is ignored ($\chi^s = 0$ and $\zeta^s = 0$), Eq.(31) can be degenerated into the solutions considering the Gurtin-Murdoch interface model.

Using strain displacement-gradient compatibility and the constitutive relations, the stress fields can be obtained easily.

5. Results and discussion

In this section, we present some numerical results to illustrate the contribution of interface elasticity with bending resistance. Due to the lack of experimental data on the values of interface bending stiffness parameters, here we use the hypothetical parameters just to demonstrate the difference between the classical results and those for the Steigmann–Ogden model.

5.1.A void embedded in an infinite matrix

The first case investigated is an infinite matrix containing a spherical void under general uniform far-field stress. The material properties for the matrix are $E^m = 71$ GPa and $\nu^m = 0.35$. The interface elastic constants are selected as $\lambda^s = 3.4939$ N/m, $\mu^s = -5.4251$ N/m and $\sigma^s = 0.5689$ N/m (Tian, 2006). The radius of the void is $R_{\text{void}} = 1$ nm.

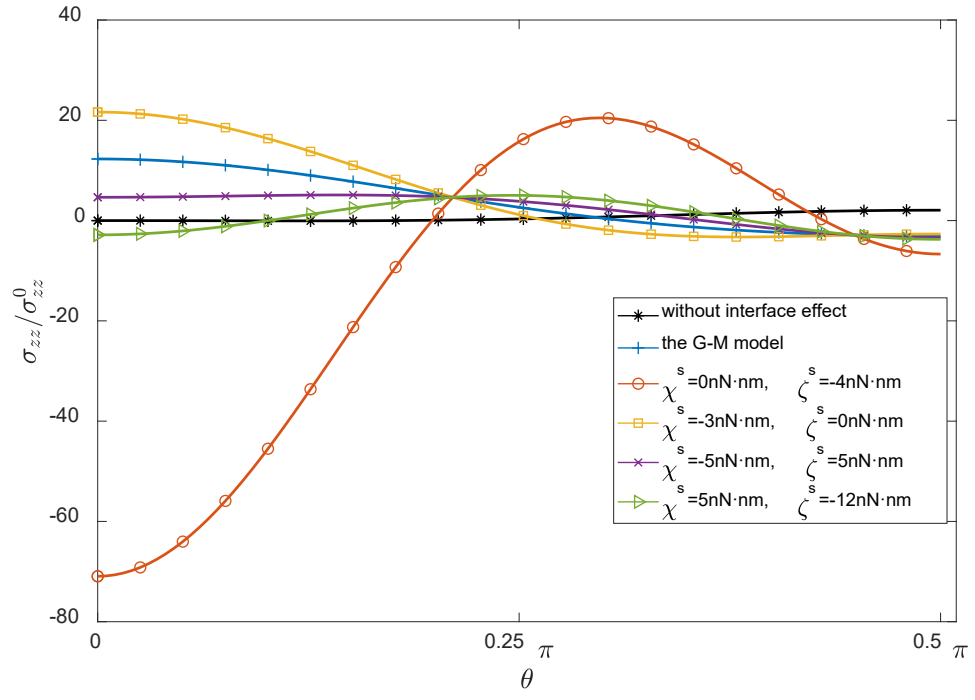
A series of parametric studies on interface properties are conducted to investigate the influence of surface bending resistance on stress distributions. Fig. 2. shows variation

of stress components along the meridian line of the void with different interface bending stiffness parameters and different type of remote loadings. From Fig. 2., we can see that stress distributions are strongly affected by the value of the interface bending stiffness parameters even when they are orders of magnitude less than materials properties constants. An interesting phenomenon is observed from Fig.2(a) that σ_{zz} with different bending stiffness parameters have the same value at the circle $\theta = \theta_{void}$ (the value of θ_{void} can be found in Appendix A) on the void surface when λ^s, μ^s and σ^s keep unchanged. It is easily found from Fig.2(a) that the maximum value of σ_{zz} is at the point $(0,0,R)$ when only $\sigma_{zz}^0 = 100\text{MPa}$ is applied. The influence of bending stiffness parameters on σ_{zz} at the point $(0,0,R)$ is further studied, as shown in Fig.3.

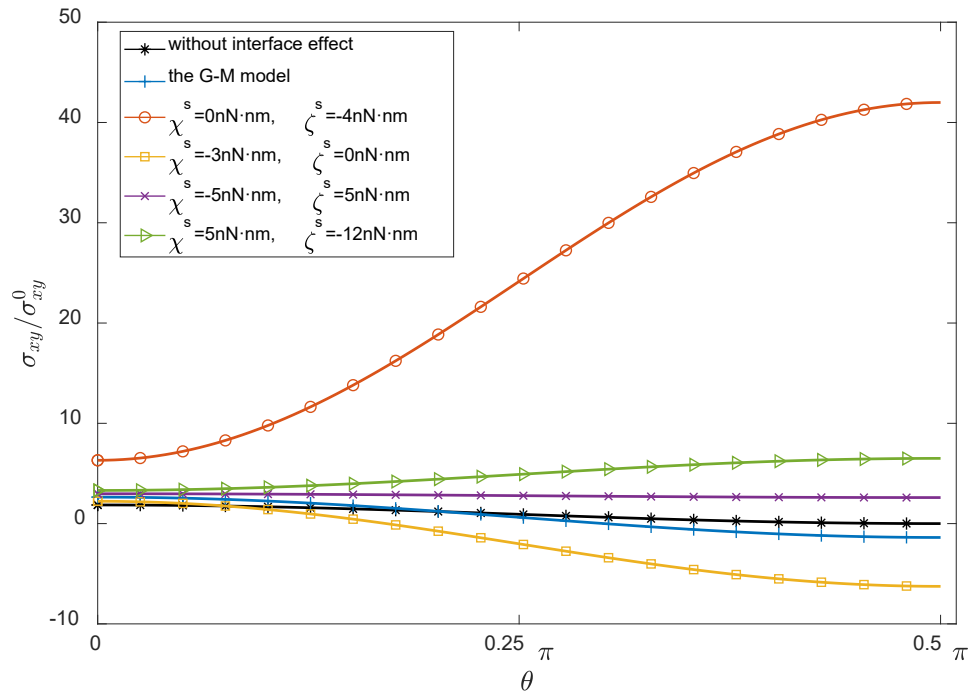
It is observed that as (χ^s, ζ^s) gets close to the characteristic line:

$$5\chi^s + 3\zeta^s + c_{void} = 0 \quad (32)$$

the stress concentration phenomenon will become quite severe, which should be avoided in the nanosized porous materials designing. The constant c_{void} is given in Appendix A. Besides, it should be pointed out that the influences of interface bending parameters on stress distribution are almost negligible when (χ^s, ζ^s) gets away from to the characteristic line.



(a)



(b)

Fig. 2. (a) Variation of σ_{zz} along the meridian line of the void for different interface

properties when $\boldsymbol{\sigma}^0 = \begin{pmatrix} 0 & 0 & 0 \\ 0 & 0 & 0 \\ 0 & 0 & 100 \end{pmatrix}$ MPa and (b) variation of σ_{xy} along the

meridian line of the void for different interface properties when

$$\boldsymbol{\sigma}^0 = \begin{pmatrix} 0 & 100 & 0 \\ 100 & 0 & 0 \\ 0 & 0 & 0 \end{pmatrix} \text{ MPa} .$$

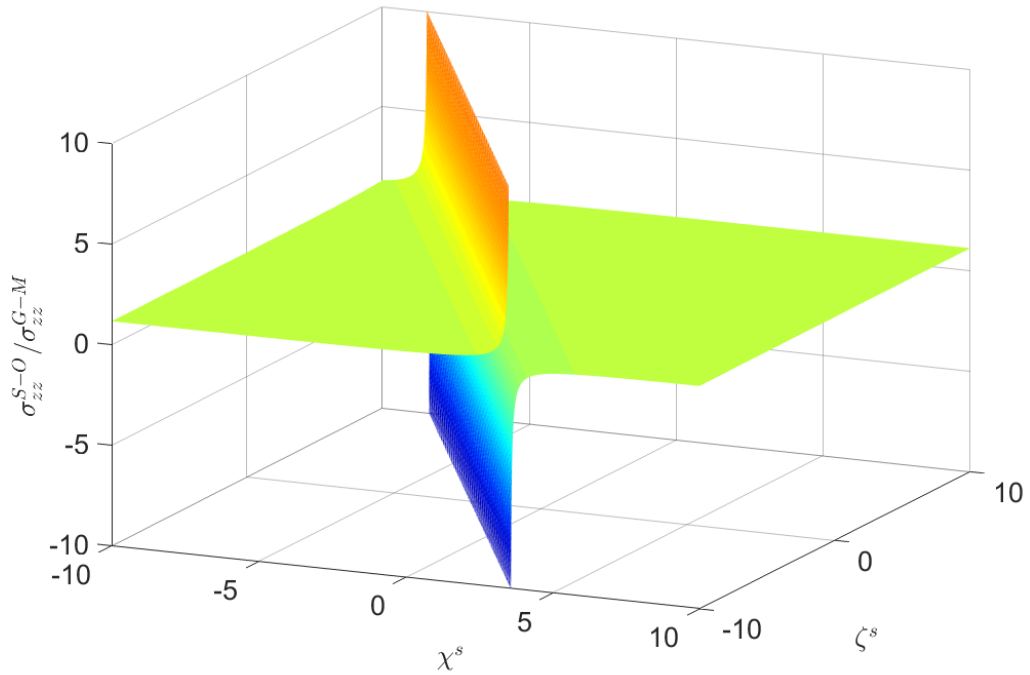


Fig. 3. The influence of χ^s and ζ^s on σ_{zz} at the point $(0,0,R)$ when

$\boldsymbol{\sigma}^0 = \begin{pmatrix} 0 & 0 & 0 \\ 0 & 0 & 0 \\ 0 & 0 & 100 \end{pmatrix}$ MPa is applied. The stress from the Steigmann–Ogden interface

model σ_{zz}^{S-O} is normalized by that from the Gurtin–Murdoch interface model σ_{zz}^{G-M} .

Fig. 4. shows $\sigma_{zz} / \sigma_{zz}^0$ at point $(0,0,R_{\text{void}})$ with different interface bending stiffness parameters and with different void radius. The results reveal that the stress is

size dependent, and such a size-dependency is influenced by the interface bending stiffness parameters. The smaller the void is, the more remarkable interface effects are.

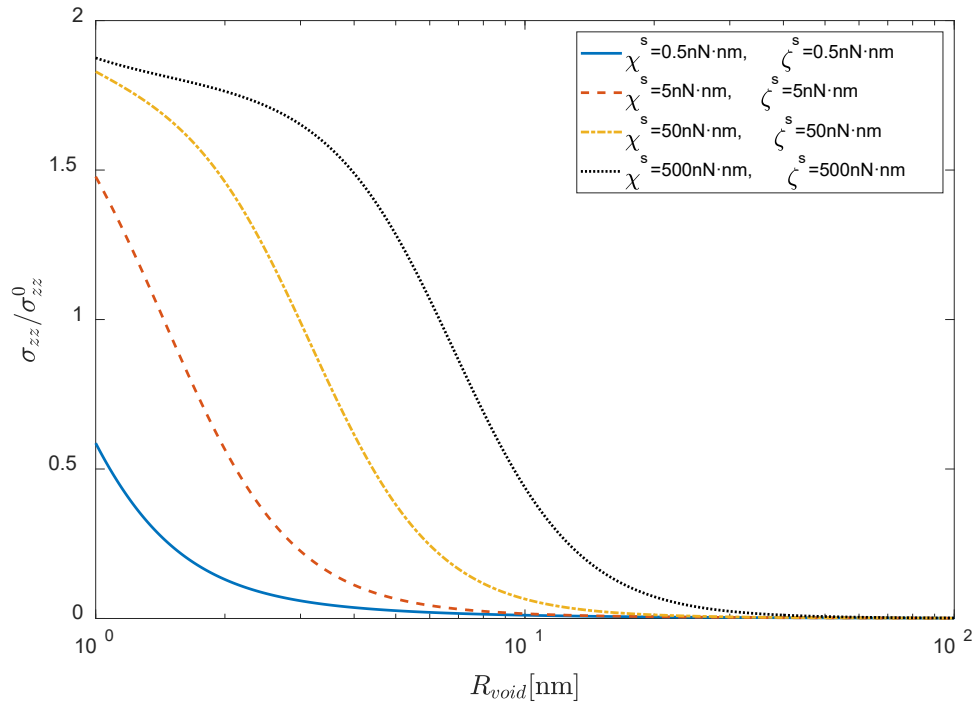


Fig. 4. Variation of $\sigma_{zz} / \sigma_{zz}^0$ at point $(0,0,R_{\text{void}})$ with the void radius for different interface properties.

5.2. An inclusion embedded in an infinite matrix

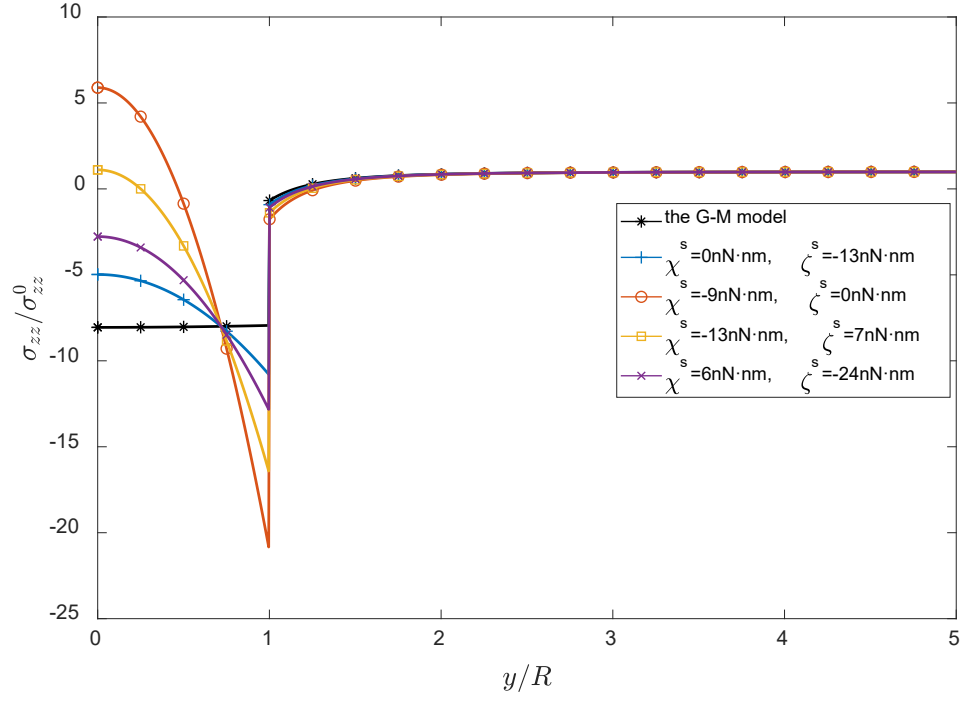
The second case investigated is an infinite matrix containing a spherical inclusion under general uniform far-field stress. The material properties for the inclusion are $E^i = 410 \text{ GPa}$ and $\nu^i = 0.14$, while the material properties for the matrix are $E^m = 71 \text{ GPa}$ and $\nu^m = 0.35$. The interface elastic constants are selected as $\lambda^s = 3.4939 \text{ N/m}$, $\mu^s = -5.4251 \text{ N/m}$ and $\sigma^s = 0.5689 \text{ N/m}$ (Tian, 2006). The radius

of the inclusion is $R_{\text{inclusion}} = 1\text{nm}$.

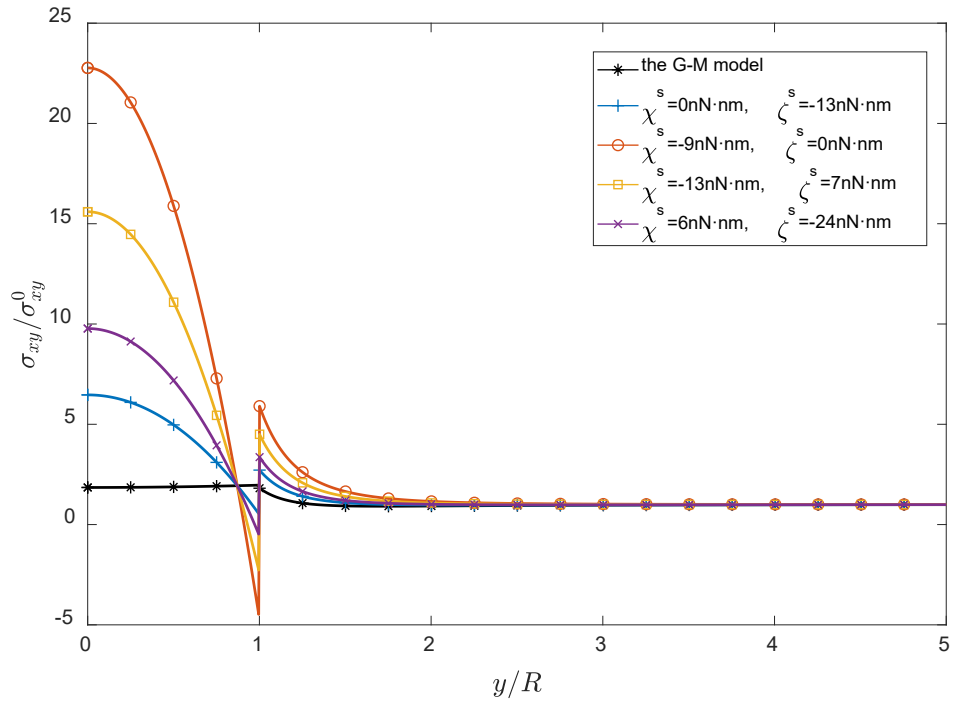
A series of parametric studies on interface properties are conducted to investigate the influence of surface bending resistance on stress distributions in vicinity of the inclusion. Fig. 5 shows variations of stress components along the line in the positive y – direction with different interface properties and different type of far-field loading. As seen from the plots, stress distributions in the inclusion with the Gurtin-Murdoch model differ a lot from the results with the Steigmann–Ogden model. The stress components with different interface bending stiffness parameters have the same value at the circle $R = R_{st}, \theta = \frac{\pi}{2}$ (the value of R_{st} is not presented in this paper because the expression for R_{st} is much too long) in the inclusion, which is similar to the void case. We also study the influence of interface stiffness parameters on the stress components at the point $(0,0,0)$ in the inclusion, as shown in Fig.6. It is easily observed that as (χ^s, ζ^s) gets close to the characteristic line:

$$5\chi^s + 3\zeta^s + c_{\text{inclusion}} = 0 \quad (33)$$

the value of σ_{zz}^i will become extremely large, which should be avoided in the nanoparticle reinforced composite designing. The constant $c_{\text{inclusion}}$ is given in Appendix A. Besides, it should be pointed out that the influences of interface bending parameters on stress distribution are almost negligible when (χ^s, ζ^s) gets away from to the characteristic line. These results reveal that the interface bending stiffness parameters can significantly change the stress distributions in the inclusion when (χ^s, ζ^s) gets closed to the characteristic line.



(a)



(b)

Fig. 5. (a) Variation of σ_{zz} along the line in the positive y -direction for different

interface properties when $\boldsymbol{\sigma}^0 = \begin{pmatrix} 0 & 0 & 0 \\ 0 & 0 & 0 \\ 0 & 0 & 100 \end{pmatrix}$ MPa and (b) variation of σ_{xy} along the

line in the positive y -direction for different interface properties when

$$\boldsymbol{\sigma}^0 = \begin{pmatrix} 0 & 100 & 0 \\ 100 & 0 & 0 \\ 0 & 0 & 0 \end{pmatrix} \text{ MPa} .$$

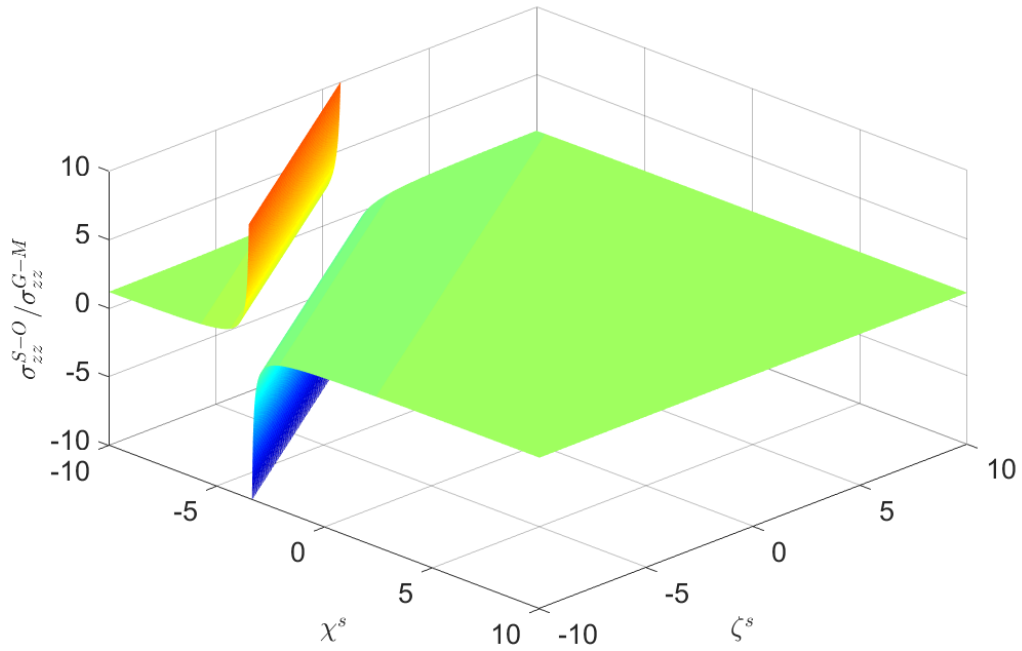


Fig. 6. The influence of χ^s and ζ^s on σ_{zz}^i at the point $(0,0,0)$ when

$$\boldsymbol{\sigma}^0 = \begin{pmatrix} 0 & 0 & 0 \\ 0 & 0 & 0 \\ 0 & 0 & 100 \end{pmatrix} \text{ MPa is applied. The stress from the Steigmann–Ogden interface}$$

model σ_{zz}^{S-O} is normalized by that from the Gurtin–Murdoch interface model σ_{zz}^{G-M}

Fig. 7. shows computed $\sigma_{zz}^i / \sigma_{zz}^0$ at point $(0, R_{\text{inclusion}}, 0)$ with different interface stiffness parameters and with different inclusion radius. The results reveal that the

interface effect caused by interface bending stiffness parameters is size dependent. The smaller the inclusion is, the more remarkable interface effects are.

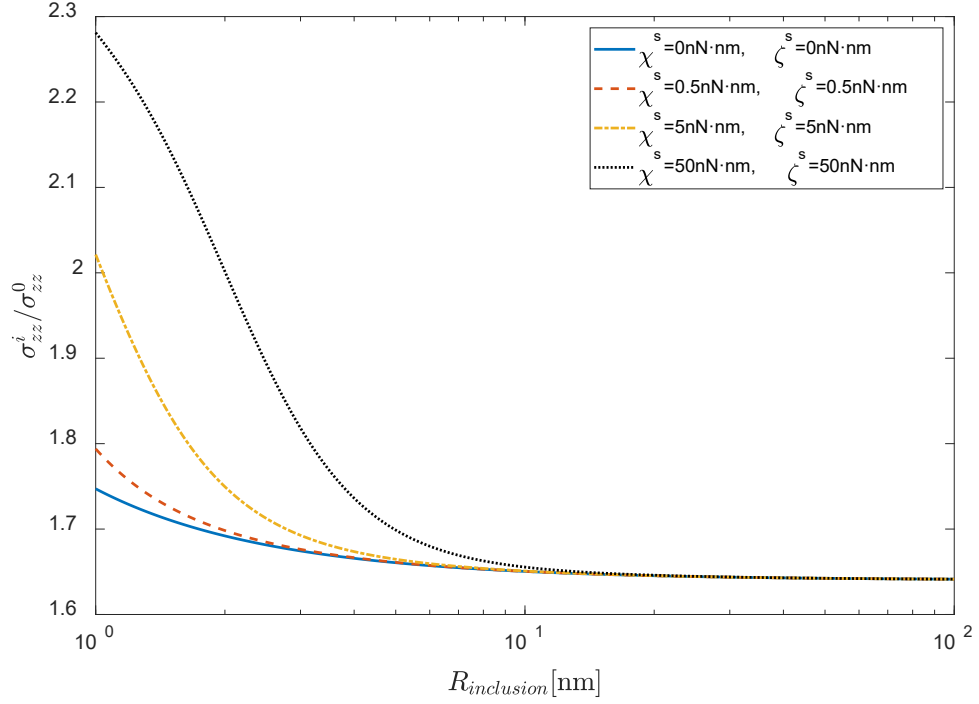


Fig. 7. $\sigma_{zz}^i / \sigma_{zz}^0$ at point $(0, R_{inclusion}, 0)$ in the inclusion with different inclusion radius

6. Conclusions

In this study, an explicit analytical solution considering interface bending resistance based on the Steigmann–Ogden interface model is derived for a spherical nano-inhomogeneity (nanoscale void/inclusion) embedded in an infinite matrix under general uniform far-field stress (including both tension and shear). A superposition technique is introduced to overcome the mathematical complexity in the Steigmann–Ogden interface model, that is the nonlinearity of the constitutive relation brought by interface residual

stress. Numerical examples show that the stress fields considering the interface bending resistance with the Steigmann–Ogden interface model, differ a lot from those considering only the interface stretching resistance with the Gurtin–Murdoch interface model.

Two interesting phenomena are observed in this study. Firstly, we observe that some stress components are invariant to interface bending stiffness parameters at a certain circle in the inclusion/matrix when interface stretch stiffness parameters are fixed values. Secondly, we present a characteristic line for interface bending stiffness parameters in this paper. If the interface bending stiffness parameters get close to the characteristic line, the stress concentration phenomenon will become quite severe, which should be avoided in the nano-composites designing.

The present explicit analytical solution derived in this paper can be used as a benchmark for numerical solutions, such as the computational grains for nanocomposites by using multi-field boundary variational principles (Dong and Atluri, 2012a; Dong and Atluri, 2012b, c).

Acknowledgement

The authors thankfully acknowledge the support from the National Key Research and Development Program of China (No. 2017YFA0207800) and the National Natural Science Foundation of China (grant No. 11872008).

Appendix A

For the case that the remote loading has only one non-zero stress component being

$\sigma_{kk}^0 (k = x, y, z)$, The dimensionless constants $M_{pkk} (p = 1, \dots, 5 \text{ and } k = x, y, z)$ and

$C_{qkk} (q = 1, 2, 3 \text{ and } k = x, y, z)$ are defined by:

$$M_{1kk} = -\frac{(-1+2v^m)\sigma_{kk}^0}{6(1+v^m)\mu^m} \quad (\text{A.1})$$

$$M_{2kk} = (R^3((-1+2v^m)((-2+4v^i)\lambda^s - R(1+v^i)\mu^i + (-1+2v^i)(2\mu^s + \sigma^s))\sigma_{kk}^0 - (-1+2v^i)(1+v^m)\mu^m(6\sigma^s - R\sigma_{kk}^0))) / (6(1+v^m)\mu^m((-2+4v^i)\lambda^s - R(\mu^i + v^i\mu^i + 2\mu^m - 4v^i\mu^m) + (-1+2v^i)(2\mu^s + \sigma^s))) \quad (\text{A.2})$$

$$M_{3kk} = \frac{\sigma_{kk}^0}{6\mu^m} \quad (\text{A.3})$$

$$M_{4kk} = -((5R^3\sigma_{kk}^0(R^4(\mu^i - \mu^m)((7+5v^i)\mu^i + 4(7-10v^i)\mu^m) - 3\zeta^s(8(-7+10v^i)\lambda^s + R(-49\mu^i + 61v^i\mu^i + 28\mu^m - 40v^i\mu^m) + 2(-7+10v^i)(10\mu^s - \sigma^s)) + R^3((35-47v^i)\lambda^s\mu^i + 4(-7+10v^i)\lambda^s\mu^m - 49(-1+v^i)\mu^i\mu^s + (35-53v^i)\mu^i\sigma^s + 6(-7+10v^i)\mu^m\sigma^s) - 2R^2(-7+10v^i)(2\mu^s(\lambda^s + \mu^s) + (\lambda^s + 5\mu^s)\sigma^s - \sigma^{s2}) - 5R((-49+61v^i)\mu^i + 4(7-10v^i)\mu^m)\chi^s - 10(-7+10v^i)(4\lambda^s + 10\mu^s - \sigma^s)\chi^s)) / (12\mu^m(-R^4((7+5v^i)\mu^i + 4(7-10v^i)\mu^m)(2(-4+5v^m)\mu^i + (-7+5v^m)\mu^m) + 6\zeta^s(8(-7+10v^i)(-4+5v^m)\lambda^s + R(-49+61v^i)(-4+5v^m)\mu^i + 4R(-7+10v^i)(-8+7v^m)\mu^m + 2(-7+10v^i)(-4+5v^m)(10\mu^s - \sigma^s)) + 4R^2(-7+10v^i)(-4+5v^m)(2\mu^s(\lambda^s + \mu^s) + (\lambda^s + 5\mu^s)\sigma^s - \sigma^{s2}) + 2R^3((-35+47v^i)(-4+5v^m)\lambda^s\mu^i + 4(-7+10v^i)(-5+4v^m)\lambda^s\mu^m + (-4+5v^m)\mu^i(49(-1+v^i)\mu^s + (-35+53v^i)\sigma^s) + 3(-7+10v^i)\mu^m(14(-1+v^m)\mu^s + (-5+3v^m)\sigma^s)) + 10R((-49+61v^i)(-4+5v^m)\mu^i + 4(-7+10v^i)(-8+7v^m)\mu^m)\chi^s + 20(-7+10v^i)(-4+5v^m)(4\lambda^s + 10\mu^s - \sigma^s)\chi^s))) \quad (\text{A.4})$$

$$\begin{aligned}
M_{5kk} = & -((R^5 \sigma_{kk}^0 (R^4 (\mu^i - \mu^m)((7 + 5v^i)\mu^i + 4(7 - 10v^i)\mu^m) - 3\zeta^s (8(-7 + 10v^i)\lambda^s + R(-49 + 61v^i)\mu^i + 4R(-7 + 10v^i)(-3 + 2v^m)\mu^m + 2(-7 + 10v^i)(10\mu^s - \sigma^s)) - 2R^2(-7 + 10v^i)(2\mu^s(\lambda^s + \mu^s) + (\lambda^s + 5\mu^s)\sigma^s - \sigma^{s2}) + R^3(\lambda^s((35 - 47v^i)\mu^i + 4(-7 + 10v^i)v^m\mu^m) + \mu^i(-49(-1 + v^i)\mu^s + 35\sigma^s - 53v^i\sigma^s) + 2(-7 + 10v^i)\mu^m(4(-1 + v^m)\mu^s + 5\sigma^s - 2v^m\sigma^s)) - 5R \\
& ((-49 + 61v^i)\mu^i + 4(-7 + 10v^i)(-3 + 2v^m)\mu^m)\chi^s - 10(-7 + 10v^i)(4\lambda^s + 10\mu^s - \sigma^s)\chi^s)) / (2\mu^m(-R^4((7 + 5v^i)\mu^i + 4(7 - 10v^i)\mu^m)(2(-4 + 5v^m)\mu^i + (-7 + 5v^m)\mu^m) + 6\zeta^s(8(-7 + 10v^i)(-4 + 5v^m)\lambda^s + R(-49 + 61v^i)(-4 + 5v^m)\mu^i + 4R(-7 + 10v^i)(-8 + 7v^m)\mu^m + 2(-7 + 10v^i)(-4 + 5v^m)(10\mu^s - \sigma^s)) + 4R^2(-7 + 10v^i)(-4 + 5v^m)(2\mu^s(\lambda^s + \mu^s) + (\lambda^s + 5\mu^s)\sigma^s - \sigma^{s2}) + 2R^3((-35 + 47v^i)(-4 + 5v^m)\lambda^s\mu^i + 4(-7 + 10v^i)(-5 + 4v^m)\lambda^s\mu^m + (-4 + 5v^m)\mu^i(49(-1 + v^i)\mu^s + (-35 + 53v^i)\sigma^s) + 3(-7 + 10v^i)\mu^m(14(-1 + v^m)\mu^s + (-5 + 3v^m)\sigma^s)) + 10R((-49 + 61v^i)(-4 + 5v^m)\mu^i + 4(-7 + 10v^i)(-8 + 7v^m)\mu^m)\chi^s + 20(-7 + 10v^i)(-4 + 5v^m)(4\lambda^s + 10\mu^s - \sigma^s)\chi^s))) \quad (A.5)
\end{aligned}$$

$$\begin{aligned}
C_{1kk} = & -(((-1 + 2v^i)(2(1 + v^m)\sigma^s + R(-1 + v^m)\sigma_{kk}^0)) / (2(1 + v^m)((-2 + 4v^i)\lambda^s - R(\mu^i + v^i\mu^i + 2\mu^m - 4v^i\mu^m) + (-1 + 2v^i)(2\mu^s + \sigma^s)))) \quad (A.6)
\end{aligned}$$

$$\begin{aligned}
C_{2kk} = & (5(-1 + v^m)\sigma_{kk}^0(6\zeta^s + R^2(-\lambda^s - 2\mu^s + \sigma^s) + 10\chi^s)) / (R(R^4((7 + 5v^i)\mu^i + 4(7 - 10v^i)\mu^m)(2(-4 + 5v^m)\mu^i + (-7 + 5v^m)\mu^m) - 6\zeta^s(8(-7 + 10v^i)(-4 + 5v^m)\lambda^s + R(-49 + 61v^i)(-4 + 5v^m)\mu^i + 4R(-7 + 10v^i)(-8 + 7v^m)\mu^m + 2(-7 + 10v^i)(-4 + 5v^m)(10\mu^s - \sigma^s)) - 4R^2(-7 + 10v^i)(-4 + 5v^m)(2\mu^s(\lambda^s + \mu^s) + (\lambda^s + 5\mu^s)\sigma^s - \sigma^{s2}) - 2R^3((-35 + 47v^i)(-4 + 5v^m)\lambda^s\mu^i + 4(-7 + 10v^i)(-5 + 4v^m)\lambda^s\mu^m + (-4 + 5v^m)\mu^i(49(-1 + v^i)\mu^s + (-35 + 53v^i)\sigma^s) + 3(-7 + 10v^i)\mu^m(14(-1 + v^m)\mu^s + (-5 + 3v^m)\sigma^s)) - 10R((-49 + 61v^i)(-4 + 5v^m)\mu^i + 4(-7 + 10v^i)(-8 + 7v^m)\mu^m)\chi^s - 20(-7 + 10v^i)(-4 + 5v^m)(4\lambda^s + 10\mu^s - \sigma^s)\chi^s)) \quad (A.7)
\end{aligned}$$

$$\begin{aligned}
C_{3kk} = & -((5R(-1+v^m)\sigma_{kk}^0(12(-7+16v^i)\zeta^s - R^3((7+5v^i)\mu^i + 4(7-10 \\
& v^i)\mu^m) + R^2(6(-7+8v^i)\lambda^s + 56(-1+v^i)\mu^s + 4(-7+13v^i)\sigma^s) + 20(-7 \\
& +16v^i)\chi^s)) / (2(R^4((7+5v^i)\mu^i + 4(7-10v^i)\mu^m)(2(-4+5v^m)\mu^i + (-7 \\
& +5v^m)\mu^m) - 6\zeta^s(8(-7+10v^i)(-4+5v^m)\lambda^s + R(-49+61v^i)(-4+5v^m) \\
& \mu^i + 4R(-7+10v^i)(-8+7v^m)\mu^m + 2(-7+10v^i)(-4+5v^m)(10\mu^s - \sigma^s) \\
&) - 4R^2(-7+10v^i)(-4+5v^m)(2\mu^s(\lambda^s + \mu^s) + (\lambda^s + 5\mu^s)\sigma^s - \sigma^{s2}) - 2R^3 \\
& ((-35+47v^i)(-4+5v^m)\lambda^s\mu^i + 4(-7+10v^i)(-5+4v^m)\lambda^s\mu^m + (-4+5v^m) \\
& \mu^i(49(-1+v^i)\mu^s + (-35+53v^i)\sigma^s) + 3(-7+10v^i)\mu^m(14(-1+v^m)\mu^s + \\
& (-5+3v^m)\sigma^s)) - 10R((-49+61v^i)(-4+5v^m)\mu^i + 4(-7+10v^i)(-8+7v^m) \\
& \mu^m)\chi^s - 20(-7+10v^i)(-4+5v^m)(4\lambda^s + 10\mu^s - \sigma^s)\chi^s))) \quad (A.8)
\end{aligned}$$

For the case that the remote loading has only one non-zero stress component being

$\sigma_{st}^0(s, t = x, y, z, s \neq t)$, The dimensionless constants M_{pst} ($p = 2, \dots, 5$ and $s, t = x, y, z$)

and C_{qst} ($q = 1, 2, 3$ and $s, t = x, y, z$) are defined by:

$$\begin{aligned}
M_{2st} = & (R^3(-1+2v^i)\sigma^s) / ((2-4v^i)\lambda^s + R(\mu^i + v^i\mu^i + 2\mu^m - 4v^i\mu^m) \\
& + 2\mu^s + \sigma^s - 2v^i(2\mu^s + \sigma^s)) \quad (A.9)
\end{aligned}$$

$$M_{3st} = \frac{\sigma_{st}^0}{6\mu^m}; \quad (A.10)$$

$$\begin{aligned}
M_{4st} = & -((5R^3\sigma_{st}^0(R^4(\mu^i - \mu^m)((7+5v^i)\mu^i + 4(7-10v^i)\mu^m) - 3\zeta^s(8(-7+10v^i)\lambda^s \\
& + R(-49\mu^i + 61v^i\mu^i + 28\mu^m - 40v^i\mu^m) + 2(-7+10v^i)(10\mu^s - \sigma^s)) + R^3((35-47v^i)\lambda^s\mu^i \\
& + 4(-7+10v^i)\lambda^s\mu^m - 49(-1+v^i)\mu^i\mu^s + (35-53v^i)\mu^i\sigma^s + 6(-7+10v^i)\mu^m\sigma^s) - 2R^2(-7+10v^i)(2\mu^s(\lambda^s + \mu^s) \\
& + (\lambda^s + 5\mu^s)\sigma^s - \sigma^{s2}) - 5R((-49+61v^i)\mu^i + 4(7-10v^i)\mu^m)\chi^s - 10(-7+10v^i)(4\lambda^s + 10\mu^s - \sigma^s)\chi^s) \\
&) / (12\mu^m(-R^4((7+5v^i)\mu^i + 4(7-10v^i)\mu^m)(2(-4+5v^m)\mu^i + (-7+5v^m)\mu^m) + 6\zeta^s(8(-7+10v^i)(-4+5v^m)\lambda^s \\
& + R(-49+61v^i)(-4+5v^m)\mu^i + 4R(-7+10v^i)(-8+7v^m)\mu^m + 2(-7+10v^i)(-4+5v^m)(10\mu^s - \sigma^s)) \\
& + 4R^2(-7+10v^i)(-4+5v^m)(2\mu^s(\lambda^s + \mu^s) + (\lambda^s + 5\mu^s)\sigma^s - \sigma^{s2}) + 2R^3((-35+47v^i)(-4+5v^m)\lambda^s\mu^i \\
& + 4(-7+10v^i)(-5+4v^m)\lambda^s\mu^m + (-4+5v^m)\mu^i(49(-1+v^i)\mu^s + (-35+53v^i)\sigma^s) + 3(-7+10v^i)\mu^m(14(-1+v^m)\mu^s \\
& + (-5+3v^m)\sigma^s)) + 10R((-49+61v^i)(-4+5v^m)\mu^i + 4(-7+10v^i)(-8+7v^m)\mu^m)\chi^s + 20(-7+10v^i)(-4+5v^m)(4\lambda^s \\
& + 10\mu^s - \sigma^s)\chi^s))) \quad (A.11)
\end{aligned}$$

$$\begin{aligned}
M_{5st} = & -((R^5 \sigma_{st}^0 (R^4 (\mu^i - \mu^m) ((7 + 5v^i) \mu^i + 4(7 - 10v^i) \mu^m) - 3\zeta^s (8(- \\
& 7 + 10v^i) \lambda^s + R(-49 + 61v^i) \mu^i + 4R(-7 + 10v^i) (-3 + 2v^m) \mu^m + 2(-7 \\
& + 10v^i) (10\mu^s - \sigma^s)) - 2R^2 (-7 + 10v^i) (2\mu^s (\lambda^s + \mu^s) + (\lambda^s + 5\mu^s) \sigma^s - \\
& \sigma^{s2}) + R^3 (\lambda^s ((35 - 47v^i) \mu^i + 4(-7 + 10v^i) v^m \mu^m) + \mu^i (-49(-1 + v^i) \mu^s \\
& + 35\sigma^s - 53v^i \sigma^s) + 2(-7 + 10v^i) \mu^m (4(-1 + v^m) \mu^s + 5\sigma^s - 2v^m \sigma^s)) - 5 \\
& R((-49 + 61v^i) \mu^i + 4(-7 + 10v^i) (-3 + 2v^m) \mu^m) \chi^s - 10(-7 + 10v^i) (4\lambda^s \\
& + 10\mu^s - \sigma^s) \chi^s)) / (2\mu^m (-R^4 ((7 + 5v^i) \mu^i + 4(7 - 10v^i) \mu^m) (2(-4 + 5v^m) \\
&) \mu^i + (-7 + 5v^m) \mu^m) + 6\zeta^s (8(-7 + 10v^i) (-4 + 5v^m) \lambda^s + R(-49 + 61v^i) (- \\
& -4 + 5v^m) \mu^i + 4R(-7 + 10v^i) (-8 + 7v^m) \mu^m + 2(-7 + 10v^i) (-4 + 5v^m) (10 \\
& \mu^s - \sigma^s)) + 4R^2 (-7 + 10v^i) (-4 + 5v^m) (2\mu^s (\lambda^s + \mu^s) + (\lambda^s + 5\mu^s) \sigma^s - \\
& \sigma^{s2}) + 2R^3 ((-35 + 47v^i) (-4 + 5v^m) \lambda^s \mu^i + 4(-7 + 10v^i) (-5 + 4v^m) \lambda^s \mu^m \\
& + (-4 + 5v^m) \mu^i (49(-1 + v^i) \mu^s + (-35 + 53v^i) \sigma^s) + 3(-7 + 10v^i) \mu^m (14(- \\
& -1 + v^m) \mu^s + (-5 + 3v^m) \sigma^s)) + 10R((-49 + 61v^i) (-4 + 5v^m) \mu^i + 4(-7 + \\
& 10v^i) (-8 + 7v^m) \mu^m) \chi^s + 20(-7 + 10v^i) (-4 + 5v^m) (4\lambda^s + 10\mu^s - \sigma^s) \chi^s))) \quad (A.12)
\end{aligned}$$

$$\begin{aligned}
C_{1st} = & (\sigma^s - 2v^i \sigma^s) / ((-2 + 4v^i) \lambda^s - R(\mu^i + v^i \mu^i + 2\mu^m - 4v^i \mu^m) + (-1 \\
& + 2v^i) (2\mu^s + \sigma^s)) \quad (A.13)
\end{aligned}$$

$$\begin{aligned}
C_{2st} = & (5(-1 + v^m) \sigma_{st}^0 (6\zeta^s + R^2 (-\lambda^s - 2\mu^s + \sigma^s) + 10\chi^s)) / (R(R^4 ((7 + \\
& 5v^i) \mu^i + 4(7 - 10v^i) \mu^m) (2(-4 + 5v^m) \mu^i + (-7 + 5v^m) \mu^m) - 6\zeta^s (8(-7 + \\
& 10v^i) (-4 + 5v^m) \lambda^s + R(-49 + 61v^i) (-4 + 5v^m) \mu^i + 4R(-7 + 10v^i) (-8 + \\
& 7v^m) \mu^m + 2(-7 + 10v^i) (-4 + 5v^m) (10\mu^s - \sigma^s)) - 4R^2 (-7 + 10v^i) (-4 + \\
& 5v^m) (2\mu^s (\lambda^s + \mu^s) + (\lambda^s + 5\mu^s) \sigma^s - \sigma^{s2}) - 2R^3 ((-35 + 47v^i) (-4 + 5v^m) \\
&) \lambda^s \mu^i + 4(-7 + 10v^i) (-5 + 4v^m) \lambda^s \mu^m + (-4 + 5v^m) \mu^i (49(-1 + v^i) \mu^s + \\
& (-35 + 53v^i) \sigma^s) + 3(-7 + 10v^i) \mu^m (14(-1 + v^m) \mu^s + (-5 + 3v^m) \sigma^s)) - \\
& 10R((-49 + 61v^i) (-4 + 5v^m) \mu^i + 4(-7 + 10v^i) (-8 + 7v^m) \mu^m) \chi^s - 20 \\
& (-7 + 10v^i) (-4 + 5v^m) (4\lambda^s + 10\mu^s - \sigma^s) \chi^s)) \quad (A.14)
\end{aligned}$$

$$\begin{aligned}
C_{3st} = & -((5R(-1+v^m)\sigma_{st}^0(12(-7+16v^i)\zeta^s - R^3((7+5v^i)\mu^i + 4(7-10 \\
& v^i)\mu^m) + R^2(6(-7+8v^i)\lambda^s + 56(-1+v^i)\mu^s + 4(-7+13v^i)\sigma^s) + 20(-7 \\
& +16v^i)\chi^s)) / (2(R^4((7+5v^i)\mu^i + 4(7-10v^i)\mu^m)(2(-4+5v^m)\mu^i + (-7 \\
& +5v^m)\mu^m) - 6\zeta^s(8(-7+10v^i)(-4+5v^m)\lambda^s + R(-49+61v^i)(-4+5v^m) \\
& \mu^i + 4R(-7+10v^i)(-8+7v^m)\mu^m + 2(-7+10v^i)(-4+5v^m)(10\mu^s - \sigma^s \\
&)) - 4R^2(-7+10v^i)(-4+5v^m)(2\mu^s(\lambda^s + \mu^s) + (\lambda^s + 5\mu^s)\sigma^s - \sigma^{s2}) - 2 \\
& R^3((-35+47v^i)(-4+5v^m)\lambda^s\mu^i + 4(-7+10v^i)(-5+4v^m)\lambda^s\mu^m + (-4 \\
& +5v^m)\mu^i(49(-1+v^i)\mu^s + (-35+53v^i)\sigma^s) + 3(-7+10v^i)\mu^m(14(-1+ \\
& v^m)\mu^s + (-5+3v^m)\sigma^s)) - 10R((-49+61v^i)(-4+5v^m)\mu^i + 4(-7+10v^i \\
&)(-8+7v^m)\mu^m)\chi^s - 20(-7+10v^i)(-4+5v^m)(4\lambda^s + 10\mu^s - \sigma^s)\chi^s))) \quad (A.15)
\end{aligned}$$

For void problem, we can get M_{pst} by setting $v_i = \mu_i = 0$ in Eqs. (A.1- A.5 and

A.9-A.12).

The other constants in this paper is given here:

$$\begin{aligned}
c_{void} = & (R^2(2R^2(-7+5v^m)\mu^{m2} + R\mu^m(4(-5+4v^m)\lambda s + 42(-1+v^m)\mu s \\
& + 3(-5+3v^m)\sigma^s) + 2(-4+5v^m)(2\mu^s(\lambda s + \mu^s) + (\lambda s + 5\mu^s)\sigma^s - \sigma^{s2}))) \quad (A.16) \\
& / (8(-4+5v^m)\lambda s + 4R(-8+7v^m)\mu^m + 2(-4+5v^m)(10\mu^s - \sigma^s))
\end{aligned}$$

$$\begin{aligned}
c_{inclusion} = & (R^2(-R^2((7+5v^i)\mu^i + 4(7-10v^i)\mu^m)(2(-4+5v^m)\mu^i + (-7 \\
& +5v^m)\mu^m) + 4(-7+10v^i)(-4+5v^m)(2\mu^s(\lambda^s + \mu^s) + (\lambda^s + 5\mu^s)\sigma^s - \sigma^{s2} \\
&) + 2R((-35+47v^i)(-4+5v^m)\lambda^s\mu^i + 4(-7+10v^i)(-5+4v^m)\lambda^s\mu^m + (\\
& -4+5v^m)\mu^i(49(-1+v^i)\mu^s + (-35+53v^i)\sigma^s) + 3(-7+10v^i)\mu^m(14(-1 \\
& +v^m)\mu^s + (-5+3v^m)\sigma^s)))) / (2(8(-7+10v^i)(-4+5v^m)\lambda^s + R(-49+61 \\
& v^i)(-4+5v^m)\mu^i + 4R(-7+10v^i)(-8+7v^m)\mu^m + 2(-7+10v^i)(-4+5v^m) \\
&)(10\mu^s - \sigma^s))) \quad (A.17)
\end{aligned}$$

$$\begin{aligned}
\theta_{\text{void}} = & \frac{1}{2} \arctan[-((\sqrt{((8(88 + (29 - 167v^m)v^m)\lambda^{s2} - 1724R^2\mu^{m2} + 3188 \\
& R^2v^m\mu^{m2} - 1424R^2v^{m2}\mu^{m2} - 7004R\mu^m\mu^s + 19568Rv^m\mu^m\mu^s - 11444R \\
& v^{m2}\mu^m\mu^s - 6936\mu^{s2} + 27132v^m\mu^{s2} - 22956v^{m2}\mu^{s2} + 3286R\mu^m\sigma^s - 6172 \\
& Rv^m\mu^m\sigma^s + 2926Rv^{m2}\mu^m\sigma^s + 7208\mu^s\sigma^s - 18296v^m\mu^s\sigma^s + 11648v^{m2}\mu^s\sigma^s \\
& - 1166\sigma^{s2} + 2597v^m\sigma^{s2} - 1421v^{m2}\sigma^{s2} + 2\lambda^s(-6R(18 + v^m(-301 + 233v^m) \\
&)\mu^m + 2(68 + (2209 - 2827v^m)v^m)\mu^s + 3(212 + v^m(-659 + 497v^m))\sigma^s) - \\
& 32\lambda^s\sqrt{(5(6(2 + (2(-2 + v^m)\lambda^s + 2R(-8 + 77v^m))\mu^m - 34\mu^s + 56v^m\mu^s + \\
& 13\sigma^s - 14v^m\sigma^s) + ((-32 + 22v^m)\lambda^s + 2R(-13 + 8v^m))\mu^m - 68\mu^s + 58v^m \\
& \mu^s + 2\sigma^s - 7v^m\sigma^s)^2) + 22v^m\lambda^s\sqrt{(5(6(2 + 3v^m)\lambda^s - 20R\mu^m + 22Rv^m\mu^m \\
& - 34\mu^s + 92v^m\mu^s + 29\sigma^s - 28v^m\sigma^s)(2(-2 + 7v^m)\lambda^s + 2R(-8 + 7v^m))\mu^m \\
& - 34\mu^s + 56v^m\mu^s + 13\sigma^s - 14v^m\sigma^s) + ((-32 + 22v^m)\lambda^s + 2R(-13 + 8v^m) \\
& \mu^m - 68\mu^s + 58v^m\mu^s + 2\sigma^s - 7v^m\sigma^s)^2) - 26R\mu^m\sqrt{(5(6(2 + 3v^m)\lambda^s - 20 \\
& R\mu^m + 22Rv^m\mu^m - 34\mu^s + 92v^m\mu^s + 29\sigma^s - 28v^m\sigma^s)(2(-2 + 7v^m)\lambda^s + \\
& 2R(-8 + 7v^m))\mu^m - 34\mu^s + 56v^m\mu^s + 13\sigma^s - 14v^m\sigma^s) + ((-32 + 22v^m) \\
& \lambda^s + 2R(-13 + 8v^m))\mu^m - 68\mu^s + 58v^m\mu^s + 2\sigma^s - 7v^m\sigma^s)^2) + 16Rv^m\mu^m \\
& \sqrt{(5(6(2 + 3v^m)\lambda^s - 20R\mu^m + 22Rv^m\mu^m - 34\mu^s + 92v^m\mu^s + 29\sigma^s - 28v^m \\
& \sigma^s)(2(-2 + 7v^m)\lambda^s + 2R(-8 + 7v^m))\mu^m - 34\mu^s + 56v^m\mu^s + 13\sigma^s - 14v^m \\
& \sigma^s) + ((-32 + 22v^m)\lambda^s + 2R(-13 + 8v^m))\mu^m - 68\mu^s + 58v^m\mu^s + 2\sigma^s - 7 \\
& v^m\sigma^s)^2) - 68\mu^s\sqrt{(5(6(2 + 3v^m)\lambda^s - 20R\mu^m + 22Rv^m\mu^m - 34\mu^s + 92v^m \\
& \mu^s + 29\sigma^s - 28v^m\sigma^s)(2(-2 + 7v^m)\lambda^s + 2R(-8 + 7v^m))\mu^m - 34\mu^s + 56v^m \\
& \mu^s + 13\sigma^s - 14v^m\sigma^s) + ((-32 + 22v^m)\lambda^s + 2R(-13 + 8v^m))\mu^m - 68\mu^s + \\
& 58v^m\mu^s + 2\sigma^s - 7v^m\sigma^s)^2) + 58v^m\mu^s\sqrt{(5(6(2 + 3v^m)\lambda^s - 20R\mu^m + 22R \\
& v^m\mu^m - 34\mu^s + 92v^m\mu^s + 29\sigma^s - 28v^m\sigma^s)(2(-2 + 7v^m)\lambda^s + 2R(-8 + 7 \\
& v^m))\mu^m - 34\mu^s + 56v^m\mu^s + 13\sigma^s - 14v^m\sigma^s) + ((-32 + 22v^m)\lambda^s + 2R(- \\
& 13 + 8v^m))\mu^m - 68\mu^s + 58v^m\mu^s + 2\sigma^s - 7v^m\sigma^s)^2) + 2\sigma^s\sqrt{(5(6(2 + 3v^m)\lambda^s \\
& - 20R\mu^m + 22Rv^m\mu^m - 34\mu^s + 92v^m\mu^s + 29\sigma^s - 28v^m\sigma^s)(2(-2 + 7v^m)\lambda^s \\
& + 2R(-8 + 7v^m))\mu^m - 34\mu^s + 56v^m\mu^s + 13\sigma^s - 14v^m\sigma^s) + ((-32 + 22v^m) \\
& \lambda^s + 2R(-13 + 8v^m))\mu^m - 68\mu^s + 58v^m\mu^s + 2\sigma^s - 7v^m\sigma^s)^2) - 7v^m\sigma^s\sqrt{(5 \\
& (6(2 + 3v^m)\lambda^s - 20R\mu^m + 22Rv^m\mu^m - 34\mu^s + 92v^m\mu^s + 29\sigma^s - 28v^m\sigma^s) \\
& (2(-2 + 7v^m)\lambda^s + 2R(-8 + 7v^m))\mu^m - 34\mu^s + 56v^m\mu^s + 13\sigma^s - 14v^m\sigma^s) + \\
& ((-32 + 22v^m)\lambda^s + 2R(-13 + 8v^m))\mu^m - 68\mu^s + 58v^m\mu^s + 2\sigma^s - 7v^m\sigma^s)^2 \\
&)) / (2(-2 + 7v^m)\lambda^s + 2R(-8 + 7v^m))\mu^m - 34\mu^s + 56v^m\mu^s + 13\sigma^s - 14v^m \\
& \sigma^s))) / (\sqrt{((2 - 7v^m)\lambda^s + R(8 - 7v^m))\mu^m + 17\mu^s - 13\sigma^s} / 2 + 7v^m(-4\mu^s + \\
&)) / (-((-32\lambda^s + 22v^m\lambda^s - 26R\mu^m + 16Rv^m\mu^m - 68\mu^s + 58v^m\mu^s + 2\sigma^s - \\
& 7v^m\sigma^s + \sqrt{(5(6(2 + 3v^m)\lambda^s - 20R\mu^m + 22Rv^m\mu^m - 34\mu^s + 92v^m\mu^s + 29\sigma^s \\
& - 28v^m\sigma^s)(2(-2 + 7v^m)\lambda^s + 2R(-8 + 7v^m))\mu^m - 34\mu^s + 56v^m\mu^s + 13\sigma^s - \\
& 14v^m\sigma^s) + ((-32 + 22v^m)\lambda^s + 2R(-13 + 8v^m))\mu^m - 68\mu^s + 58v^m\mu^s + 2\sigma^s \\
& - 7v^m\sigma^s)^2)) / (2(-2 + 7v^m)\lambda^s + 2R(-8 + 7v^m))\mu^m - 34\mu^s + 56v^m\mu^s + 13\sigma^s \\
& - 14v^m\sigma^s)))] \tag{A.18}
\end{aligned}$$

Appendix B

In Appendix B, a brief introduction to the deduction process is presented.

First of all, we give a brief introduction to the Papkovich-Neuber potentials used in this paper. Substitute Eq.(20) into Eq.(16), and we can obtain the n -th ($n \geq 0$) order positive Papkovich-Neuber potentials. For example, the 0th order positive Papkovich-Neuber potentials can be written as:

$$\alpha_0 = \frac{1}{\mu^j \sqrt{\pi}} \begin{pmatrix} 1-v^j & 0 & 0 \\ 0 & 1-v^j & 0 \\ 0 & 0 & 1-v^j \end{pmatrix} \quad (\text{B.1})$$

The 1st order positive Papkovich-Neuber potentials can be written as:

$$\alpha_1 = \frac{\sqrt{\frac{3}{2\pi}}}{8\mu^j} \begin{pmatrix} r(-5+4v^j)\cos[\theta] & 0 & r(-5+4v^j)\sin[\theta]\sin[\varphi] \\ 0 & r(-5+4v^j)\cos[\theta] & r(5-4v^j)\cos[\varphi]\sin[\theta] \\ r(5-4v^j)\cos[\varphi]\sin[\theta] & r(5-4v^j)\sin[\theta]\sin[\varphi] & 0 \\ -2\sqrt{2}r\cos[\varphi]\sin[\theta] & 2r\cos[\varphi]\sin[\theta] & 0 \\ -2\sqrt{2}r\sin[\theta]\sin[\varphi] & 8r(-1+v^j)\sin[\theta]\sin[\varphi] & r(-5+4v^j)\cos[\theta] \\ -8\sqrt{2}r(-1+v^j)\cos[\theta] & 2r\cos[\theta] & r(-5+4v^j)\sin[\theta]\sin[\varphi] \\ 8r(-1+v^j)\cos[\varphi]\sin[\theta] & r(-5+4v^j)\sin[\theta]\sin[\varphi] & r(-5+4v^j)\cos[\theta] \\ 2r\sin[\theta]\sin[\varphi] & r(-5+4v^j)\cos[\varphi]\sin[\theta] & 0 \\ 2r\cos[\theta] & 0 & r(-5+4v^j)\cos[\varphi]\sin[\theta] \end{pmatrix} \quad (\text{B.2})$$

It should be pointed out that n -st order positive Papkovich-Neuber potentials is a $3 \times 3(2n+1)$ order matrix. Higher order positive Papkovich-Neuber potentials are not listed here, but listed in the supplement material, because they are much too long.

Substitute Eq.(21) into Eq.(15), and we can obtain the n -th ($n < 0$) order negative Papkovich-Neuber potentials. For example, the 1st order negative Papkovich-

Neuber potentials can be written as:

$$\mathbf{a}_{-1} = \frac{1}{4\mu^j\sqrt{\pi r}} \begin{pmatrix} 4 - 4\nu^j - \cos[\theta]^2 \cos[\varphi]^2 - \sin[\varphi]^2 \\ \frac{1}{2} \sin[\theta]^2 \sin[2\varphi] \\ \cos[\theta] \cos[\varphi] \sin[\theta] \\ \frac{1}{2} \sin[\theta]^2 \sin[2\varphi] & \cos[\theta] \cos[\varphi] \sin[\theta] \\ 4 - 4\nu^j - \cos[\varphi]^2 - \cos[\theta]^2 \sin[\varphi]^2 & \cos[\theta] \sin[\theta] \sin[\varphi] \\ \cos[\theta] \sin[\theta] \sin[\varphi] & \frac{1}{2} (7 - 8\nu^j + \cos[2\theta]) \end{pmatrix} \quad (\text{B.3})$$

It should be pointed out that n-st order negative Papkovitch-Neuber potentials is a $3 \times 3(2n+1)$ order matrix. Higher order negative Papkovitch-Neuber potentials are not listed here, but listed in the supplement material, because they are much too long.

The displacement field in the matrix/inclusion can be expressed as a combination of the obtained Papkovitch-Neuber potentials:

$$\begin{aligned} \mathbf{u}^m &= [\mathbf{a}_p \quad \mathbf{a}_{p+1} \quad \cdots \quad \mathbf{a}_{q-1} \quad \mathbf{a}_q] \mathbf{x} \\ \mathbf{u}^i &= [\mathbf{a}_0 \quad \mathbf{a}_1 \quad \cdots \quad \mathbf{a}_{t-1} \quad \mathbf{a}_t] \mathbf{y} \end{aligned} \quad (\text{B.4})$$

where \mathbf{x} and \mathbf{y} are the unknown coefficient vector. For spherical inhomogeneity problems, only $\mathbf{a}_{-4}, \mathbf{a}_{-2}, \mathbf{a}_0, \mathbf{a}_1$ are needed for the matrix, and $\mathbf{a}_1, \mathbf{a}_3$ are needed for the inhomogeneity. Using the strain displacement-gradient compatibility and the constitutive relations, the stress fields can be obtained easily. The stress field correspond to $\mathbf{a}_{-4}, \mathbf{a}_{-2}, \mathbf{a}_0$ is zero at infinity, and the stress field correspond to \mathbf{a}_1 is a constant matrix:

$$\sigma_1 = \frac{1}{2} \sqrt{\frac{3}{2\pi}} \begin{pmatrix} 0 & 0 & 0 & \sqrt{2}(-1+2v^j) & 1-2v^j \\ 0 & 0 & 0 & \sqrt{2}(-1+2v^j) & 2(-2+v^j) \\ 0 & 0 & 0 & -2\sqrt{2}(-2+v^j) & 1-2v^j \\ 0 & 0 & 0 & 0 & 0 \\ 0 & 0 & 0 & 0 & 0 \\ 0 & 0 & 0 & 0 & 0 \\ 0 & 2(-2+v^j) & 0 & 0 & \\ 0 & 1-2v^j & 0 & 0 & \\ 0 & 1-2v^j & 0 & 0 & \\ 0 & 0 & -\frac{5}{2}+2v^j & 0 & \\ -\frac{5}{2}+2v^j & 0 & 0 & 0 & \\ 0 & 0 & 0 & -\frac{5}{2}+2v^j & \end{pmatrix} \quad (B.5)$$

From Eq.(B.5), we can easily determine the coefficients of α_1 by satisfying the Eq.(4), which is the far field traction boundary conditions. The other coefficients in Eq.(B.4) can be determined by enforcing the interface condition described by Eqs.(5-12). The solving process is complex and tedious, and the coefficients of Papkovitch-Neuber potentials are rather complex, thus are not given in this paper. After the coefficients are determined, we substitute these coefficients into Eq.(B.4) and simplify the obtained expression. Finally, the displacement fields in matrix/inhomogeneity is simplified as Eqs.(23-28).

References

- Altenbach, H., Eremeev, V.A., Morozov, N.F., 2010. On equations of the linear theory of shells with surface stresses taken into account. *Mechanics of Solids* 45, 331-342.
- Altenbach, H., Eremeyev, V.A., 2011. On the shell theory on the nanoscale with surface stresses. *International Journal of Engineering Science* 49, 1294-1301.
- Altenbach, H., Eremeyev, V.A., Morozov, N.F., 2012. Surface viscoelasticity and effective properties of thin-walled structures at the nanoscale. *International Journal of Engineering Science* 59, 83-89.
- Altenbach, H., Eremeyev, V.A., Morozov, N.F., 2013a. On the Influence of Residual Surface Stresses on the Properties of Structures at the Nanoscale, in: Altenbach, H., Morozov, N.F. (Eds.), *Surface Effects in Solid Mechanics: Models, Simulations and Applications*. Springer Berlin Heidelberg, Berlin, Heidelberg, pp. 21-32.
- Altenbach, H., Eremeyev, V.A., Morozov, N.F., 2013b. On the influence of residual surface stresses on the properties of structures at the nanoscale, *Surface Effects in Solid Mechanics*. Springer, pp. 21-32.
- Ansari, R., Norouzzadeh, A., 2016. Nonlocal and surface effects on the buckling behavior of functionally graded nanoplates: An isogeometric analysis. *Physica E: Low-Dimensional Systems and Nanostructures* 84, 84-97.
- Ansari, R., Pourashraf, T., Gholami, R., 2015. An exact solution for the nonlinear forced vibration of functionally graded nanobeams in thermal environment based on surface elasticity theory. *Thin-Walled Structures* 93, 169-176.
- Ansari, R., Sahmani, S., 2011. Surface stress effects on the free vibration behavior of nanoplates. *International Journal of Engineering Science* 49, 1204-1215.
- Chhapadia, P., Mohammadi, P., Sharma, P., 2011. Curvature-dependent surface energy and implications for nanostructures. *Journal of the Mechanics and Physics of Solids* 59, 2103-2115.
- Diao, J., Gall, K., Dunn, M.L., 2003. Surface-stress-induced phase transformation in metal nanowires. *Nature Materials* 2, 656-660.
- Dong, C.Y., Pan, E., 2011. Boundary element analysis of nanoinhomogeneities of arbitrary shapes with surface and interface effects. *Engineering Analysis with Boundary Elements* 35, 996-1002.
- Dong, L., Wang, J., Yan, P., Guo, Z., 2018. A Trefftz collocation method for multiple interacting spherical nano-inclusions considering the interface stress effect. *Engineering Analysis with Boundary Elements* 94, 172-183.
- Dryburgh, G., Ogden, R.W., 1999. Bifurcation of an elastic surface-coated incompressible isotropic elastic block subject to bending. *Z. Angew. Math. Phys.* 50, 822-838.
- Duan, H.L., Wang, J., Karihaloo, B.L., 2009. *Theory of Elasticity at the Nanoscale*. *Advances in Applied Mechanics* 42, 1-68.

- Eltaher, M.A., Mahmoud, F.F., Assie, A.E., Meletis, E.I., 2013. Coupling effects of nonlocal and surface energy on vibration analysis of nanobeams. *Applied Mathematics and Computation* 224, 760-774.
- Eremeyev, V.A., Altenbach, H., Morozov, N.F., 2009. The influence of surface tension on the effective stiffness of nanosize plates. *Doklady Physics* 54, 98-100.
- Eremeyev, V.A., Lebedev, L.P., 2016. Mathematical study of boundary-value problems within the framework of Steigmann–Ogden model of surface elasticity. *Continuum Mechanics and Thermodynamics* 28, 407-422.
- Feng, Y., Liu, Y., Wang, B., 2010. Finite element analysis of resonant properties of silicon nanowires with consideration of surface effects. *Acta Mechanica* 217, 149-155.
- Gharahi, A., Schiavone, P., 2018. Effective elastic properties of plane micropolar nanocomposites with interface flexural effects. *International Journal of Mechanical Sciences* 149, 84-92.
- Gibbs, J.W., 1906. *The scientific papers of J. Willard Gibbs*. Longmans, Green.
- Gurtin, M., Weissmüller, J., Larche, F., 1998. A general theory of curved deformable interfaces in solids at equilibrium. *Philosophical Magazine A* 78, 1093-1109.
- Gurtin, M.E., Murdoch, A.I., 1975. A continuum theory of elastic material surfaces. *Archive for Rational Mechanics & Analysis* 57, 291-323.
- Gurtin, M.E., Murdoch, A.I., 1978. Surface stress in solids. *International Journal of Solids & Structures* 14, 431-440.
- Han, Z., Mogilevskaya, S.G., Schillinger, D., 2018. Local fields and overall transverse properties of unidirectional composite materials with multiple nanofibers and Steigmann–Ogden interfaces. *International Journal of Solids and Structures* 147, 166-182.
- He, J., Lilley, C.M., 2008. Surface effect on the elastic behavior of static bending nanowires. *Nano Letters* 8, 1798-1802.
- He, L.H., Li, Z.R., 2006. Impact of surface stress on stress concentration. *International Journal of Solids and Structures* 43, 6208-6219.
- Kushch, V.I., Mogilevskaya, S.G., Stolarski, H.K., Crouch, S.L., 2011. Elastic interaction of spherical nanoinhomogeneities with Gurtin–Murdoch type interfaces. *Journal of the Mechanics and Physics of Solids* 59, 1702-1716.
- Kushch, V.I., Mogilevskaya, S.G., Stolarski, H.K., Crouch, S.L., 2013. Elastic fields and effective moduli of particulate nanocomposites with the Gurtin–Murdoch model of interfaces. *International Journal of Solids and Structures* 50, 1141-1153.
- Li, X., Mi, C., 2018. Nanoindentation hardness of a Steigmann–Ogden surface bounding an elastic half-space. *Mathematics and Mechanics of Solids*.
- Lim, C.W., Li, Z.R., He, L.H., 2006. Size dependent, non-uniform elastic field inside a nano-scale spherical inclusion due to interface stress. *International Journal of Solids and Structures* 43, 5055-5065.
- Lu, T.Q., Zhang, W.X., Wang, T.J., 2011. The surface effect on the strain energy release rate of buckling delamination in thin film-substrate systems. *International Journal of Engineering Science* 49, 967-975.

- Lurie, A.I., 2005. Three-dimensional problems in the theory of elasticity, Theory of Elasticity. Springer Berlin Heidelberg, Berlin, Heidelberg, pp. 243-407.
- Manav, M., Anilkumar, P., Phani, A.S., 2018. Mechanics of polymer brush based soft active materials— theory and experiments. *Journal of the Mechanics and Physics of Solids* 121, 296-312.
- McDowell, M.T., Leach, A.M., Gall, K., 2008. Bending and tensile deformation of metallic nanowires. *Modelling and Simulation in Materials Science and engineering* 16, 045003.
- Medasani, B., Park, Y.H., Vasiliev, I., 2007. Theoretical study of the surface energy, stress, and lattice contraction of silver nanoparticles. *Physical Review B* 75.
- Mi, C., 2018. Elastic behavior of a half-space with a Steigmann–Ogden boundary under nanoscale frictionless patch loads. *International Journal of Engineering Science* 129, 129-144.
- Mi, C., Kouris, D., 2014. On the significance of coherent interface effects for embedded nanoparticles. *Mathematics and Mechanics of Solids* 19, 350-368.
- Miller, R.E., Shenoy, V.B., 2000a. Size-dependent elastic properties of nanosized structural elements. *Nanotechnology* 11, 139.
- Miller, R.E., Shenoy, V.B., 2000b. Size-dependent elastic properties of nanosized structural elements. *Nanotechnology* 11, 139-147.
- Mogilevskaya, S.G., Crouch, S.L., La Grotta, A., Stolarski, H.K., 2010. The effects of surface elasticity and surface tension on the transverse overall elastic behavior of unidirectional nano-composites. *Composites Science and Technology* 70, 427-434.
- Mogilevskaya, S.G., Crouch, S.L., Stolarski, H.K., 2008. Multiple interacting circular nano-inhomogeneities with surface/interface effects. *Journal of the Mechanics and Physics of Solids* 56, 2298-2327.
- Nazarenko, L., Stolarski, H., Altenbach, H., 2016. Effective properties of short-fiber composites with Gurtin-Murdoch model of interphase. *International Journal of Solids and Structures* 97-98, 75-88.
- Neuber, H.v., 1934. Ein neuer ansatz zur lösung räumlicher probleme der elastizitätstheorie. der hohlkegel unter einzellast als beispiel. *ZAMM-Journal of Applied Mathematics and Mechanics/Zeitschrift für Angewandte Mathematik und Mechanik* 14, 203-212.
- Ogden, R.W., Steigmann, D.J., Haughton, D.M., 1997. The Effect of Elastic Surface Coating on the Finite Deformation and Bifurcation of a Pressurized Circular Annulus. *J Elast* 47, 121-145.
- Papkovich, P., 1932. Solution générale des équations différentielles fondamentales d'élasticité exprimée par trois fonctions harmoniques. *CR Acad. Sci. Paris* 195, 513-515.
- Rouhi, H., Ansari, R., Darvizeh, M., 2016. Size-dependent free vibration analysis of nanoshells based on the surface stress elasticity. *Applied Mathematical Modelling* 40, 3128-3140.
- Sahmani, S., Aghdam, M.M., Akbarzadeh, A.H., 2016. Size-dependent buckling and

postbuckling behavior of piezoelectric cylindrical nanoshells subjected to compression and electrical load. *Materials and Design* 105, 341-351.

Sharma, P., Ganti, S., Bhate, N., 2003. Effect of surfaces on the size-dependent elastic state of nano-inhomogeneities. *Applied Physics Letters* 82, 535-537.

Slobodyansky, M., 1954. General forms of solution of equations of elasticity for simply connected and multiply connected domains expressed in terms of harmonic functions. *Prikl. Mat. Mekh* 18, 55-74.

Steigmann, D.J., Ogden, R.W., 1999. Elastic surface—substrate interactions. *Proceedings of the Royal Society of London. Series A: Mathematical, Physical and Engineering Sciences* 455, 437-474.

Tian, L., Rajapakse, R.K.N.D., 2007. Finite element modelling of nanoscale inhomogeneities in an elastic matrix. *Computational Materials Science* 41, 44-53.

Youcef, D.O., Kaci, A., Benzair, A., Bousahla, A.A., Tounsi, A., 2018. Dynamic analysis of nanoscale beams including surface stress effects. *Smart Structures and Systems* 21, 65-74.

Yun, G., Park, H.S., 2009. Surface stress effects on the bending properties of fcc metal nanowires. *Physical Review B* 79, 195421.

Yvonnet, J., Mitrushchenkov, A., Chambaud, G., He, Q.C., 2011. Finite element model of ionic nanowires with size-dependent mechanical properties determined by ab initio calculations. *Computer Methods in Applied Mechanics and Engineering* 200, 614-625.

Zemlyanova, A.Y., 2017. A straight mixed mode fracture with the Steigmann-Ogden boundary condition. *Q J Mech Appl Math* 70, 65-86.

Zemlyanova, A.Y., 2018a. An Adhesive Contact Problem for a Semi-plane with a Surface Elasticity in the Steigmann-Ogden Form. *J Elast.*

Zemlyanova, A.Y., 2018b. Frictionless contact of a rigid stamp with a semi-plane in the presence of surface elasticity in the Steigmann–Ogden form. *Mathematics and Mechanics of Solids* 23, 1140-1155.

Zemlyanova, A.Y., Mogilevskaya, S.G., 2018a. Circular inhomogeneity with Steigmann–Ogden interface: Local fields, neutrality, and Maxwell's type approximation formula. *International Journal of Solids and Structures* 135, 85-98.

Zemlyanova, A.Y., Mogilevskaya, S.G., 2018b. On spherical inhomogeneity with Steigmann-Ogden interface. *J Appl Mech Trans ASME* 85.

Zhao, T., Luo, J., Xiao, Z., 2015. Buckling analysis of a nanowire lying on Winkler-Pasternak elastic foundation. *Mech. Adv. Mater. Struct.* 22, 394-401.

Zhao, X.J., Rajapakse, R.K.N.D., 2013. Elastic field of a nano-film subjected to tangential surface load: Asymmetric problem. *European Journal of Mechanics, A/Solids* 39, 69-75.